VŠB – Technical University of Ostrava

Faculty of Electrical Engineering and Computer Science

Department of Applied Mathematics

Dynamics of the human cell model

Dynamika modelu lidské buňky

2018 Radek Halfar

VŠB - Technical University of Ostrava
Faculty of Electrical Engineering and Computer Science
Department of Applied Mathematics

Diploma Thesis Assignment

Ing. Radek Halfar

Student:

Study Programme: N2647 Information and Communication Technology

Study Branch: 1103T031 Computational Mathematics

Title: Dynamics of the human cell model

                         Dynamika modelu lidské buňky

The thesis language: English

Description:

There are several possibilities how to describe behavior of a given dynamical system. It is possible to describe given models by differential equations and to study their dynamical properties.

The main aim of the thesis is the study of differential equations and their dynamics, mainly models like Fenton-Karma and FitzHugh–Nagumo, using new methods (e.g. 0-1 test for chaos).

The tools for the thesis:
1. study basic notions and properties,
2. application of given techniques on models of the Fenton-Karma and FitzHugh–Nagumo type,
3. implementation of methods for detecting of dynamical properties,
4. testing of methods on given differential equations,
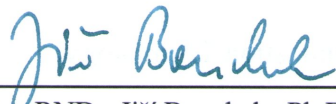5. conclusions.

References:

[1] D.W. Jordan and P. Smith, Nonlinear ordinary differential equations an introduction for scientists and engineers, Oxford GB, 2011
[2] F. Fenton and A. Karma, Vortex dynamics in three-dimensional continuous myocardium with fiber rotation: Filament instability and fibrillation. Chaos: An Interdisciplinary Journal of Nonlinear Science. 1998, 8(1), 20-47
[3] M. Krupa and J.D. Touboul, Complex Oscillations in the Delayed FitzHugh–Nagumo Equation: Filament instability and fibrillation. Journal of Nonlinear Science. 2016, 26(1), 43-81
[4] R. FitzHugh, Impulses and Physiological States in Theoretical Models of Nerve Membrane. Biophysical Journal. 1961;1(6):445-466.
[5] S. Lynch, Dynamical systems with Applications using Matlab, Birkhauser, 2004, ISBN: 0-8176-4321-4

Extent and terms of a thesis are specified in directions for its elaboration that are opened to the public on the web sites of the faculty.

Supervisor: **doc. RNDr. Marek Lampart, Ph.D.**

Date of issue: 01.09.2017

Date of submission: 30.04.2018

doc. RNDr. Jiří Bouchala, Ph.D.
Head of Department

prof. Ing. Pavel Brandštetter, CSc.
Dean

I hereby declare that this master's thesis was written by myself. I have quoted all the references I have drawn upon.

In Ostrava April 30, 2018

Abstrakt

Srdce je komplexní orgán na jehož průběžné práci je závislý život každého člověka. Jedná se o dutý svalový orgán, jehož mechanická práce je řízena elektrickými signály. Tyto signály jsou produkovány samotným srdcem a jsou šířeny různou rychlostí v jeho jednotlivých částech.

Porušení tohoto systému může vést k život ohrožujícím stavům. Je proto velmi důležité podrobně popsat tento systém, zkoumat jeho změny a účinky těchto změn na jeho funkci.

V této práci je pro aproximaci buněk srdečního svalu použit vylepšený model Fenton-Karma. Tento model je stimulován různou stimulační frekvencí a amplitudou. Odpovědi tohoto modelu jsou studovány z dynamického hlediska pomocí fázových portrétů, Fourierových spekter, Poincarého řezu, bifurkačního diagramu a testu 0-1 chaosu.

Klíčová slova: model srdeční buňky, fázový portrét, Fourierovy spektra, Poincarého řez, bifurkace, 0-1 test chaosu

Abstract

The heart is a complex organ on its continuous work is dependending life of every human. It is a hollow muscular organ whose mechanical work is controlled by electrical signals. These signals are produced by the heart itself and are propagated at different speeds at its individual parts.

Violations of this system can lead to life threatening states. It is therefore very important to describe this system in detail, examine its changes and the effects of these changes on the function of heart.

In this work, improved Fenton-Karma model is used for approximation cardiac muscle cell. This model is stimulated on various stimulation frequencies and amplitudes. Responses of this model are studied from the dynamical point of view using phase portraits, the Fourier spectra, Poincaré section, bifurcation diagram and the 0-1 test for chaos.

Key Words: cardiac cell model, phase portrait, Fourier spectra, Poincaré section, bifurcation, the 0-1 test for chaos

Contents

List of symbols and abbreviations

FK3V	–	Fenton-Karma 3 variable
SA	–	sinoatrial
AV	–	atrioventricular
APD	–	action potential duration
CV	–	conduction velocity
BR	–	Beeler-Reuter
PPI	–	postpacing interval
TCL	–	tachycardia cycle length
MSD	–	mean-square displacement
FFT	–	Fast Fourier transform

List of Figures

List of Tables

Listings

1 Introduction

Since the ischaemic heart disease is the most common cause of death in the world [4], understanding of proper heart work and effect of changes to it's work is crucial. On the mechanical work of heart depends life of every human been. This mechanical work is govern by electric system of heart. It is complex system with several stages of protection against failure. Electric signals are propagated through the heart with different speed in every region of heart. For proper propagation of this signal, special cells are created at the heart to generate and propagate electric signals - the conduction system of the heart. Signal propagation takes place not only through this system, but also through one muscle cell to the other.

In this work dynamical properties of cardiac muscle cell is described. For this purpose improvement of the well-known cardiac cell model is presented. Advantage of proposed modification is that it can better replicate shape of action potential than original model. Using this model, the response of the cell to the various stimulation frequencies and amplitudes is then simulated. These responses are studied from dynamical point of view using phase portraits, the Fourier spectra, Poincaré section, bifurcation diagram and the 0-1 test for chaos. With these tools, chaotic as well as regular responses are detected.

This thesis is organized as follows. In Section 2 a brief introduction to the heart electrophysiology is presented. Section 3 is dedicated to generalities about heart cell modeling. Section 4 describes FK3V model and it's improvement and examples of it's using. In Section 5 a brief introduction to numerical methods for examining the behavior of dynamic systems is given. In Section 6 the 0-1 test for chaos is introduced. Section 7 summarizes main results achieved in this work. Section 8 summarizes main parts of codes provided for calculation made in this thesis. Thesis is closed by conclusions in Section 9. In Appendix is attached article summarizing the main results achieved in this work. This article was accepted for publication in the journal *Mathematical Methods in the Applied Sciences* ranking Q2 (108/255) in Mathematics, Applied (2016) with impact factor 1.017 (2016).

2 Electrophysiology of the heart

2.1 The conduction system of the heart

The heart conduction system (its layout can be seen on Figure 2.1) is a very sophisticated system that tries to protect itself from the failure of its individual subsystems. From the specialized muscle cells, a sinus node (sinoatrial or SA node) is located in the right atrium at the superior vena cava. The human SA node is crescent-shaped and is about 15 mm long and 5 mm wide and its function is to be heart pacemaker. Cells of SA node are self-excitatory with frequency about 70 per minute and from sinus node activation propagates throughout the atria. At the boundary between the atria and ventricles is placed the atrioventricular node (AV node) with its inherent rate approximately 50 beats per minute. Nevertheless, when the AV node is triggered at a higher frequency, it follows this higher frequency. In healthy heart has therefore AV node only conducting function and stimulation is provided by SA node.

From AV node to the ventricle is propagation provided using specialized conduction system. Proximally is this system composed of a common bundle, called the bundle of His. This bundle is more distally separates into right and left bundle branches that spread along each side of the septum. Even more distally is conducting system further divided into Purkinje fibers, which extend on the inner sides of the heart ventricles walls. Due to the many activation sites in the inner side of the ventricular wall, the formation of a wavefront is caused. This wavefront propagetes though the ventriculi toward the outer wall. Due to the many activation sites in the inner side of the ventricular wall, the formation of a wavefront is caused. This wavefront propagetes though the ventriculi toward the outer wall. This process is due to the fact, that cardiac muscle cell (unlike skeletal muscles) can propagate action potential from one cell to another in any direction. As a result, the activation wavefronts are of rather complex shape. After depolarization of each ventricular muscle region, repolarization happens [1].

2.2 Cardiac muscle cell electrophysiology

The cardiac action potential can be recorded by microelectrodes. The typical resting potential is -80 to -90 mV (with respect to the surrounding extracellular fluid, similar to the nervous and skeletal muscle). However, since the duration of the action potential is much longer than that of the neuron and skeletal muscle, the shape of this potential is unique (see Figure 2.2). The total duration of the action potential is 200 to 300 ms (in the case of neurons and skeletal muscle cells, the action potential duration is 1 to 2 ms). The typical action potential is divided into 5 phases (as can be seen in Figure 2.2). In the initial phase (phase 0), there is a rapid increase in the action potential from a resting value to around +20 mV triggered by the inflow of sodium ions across the cell membrane (similar to other cells). In phase 1, a potential value
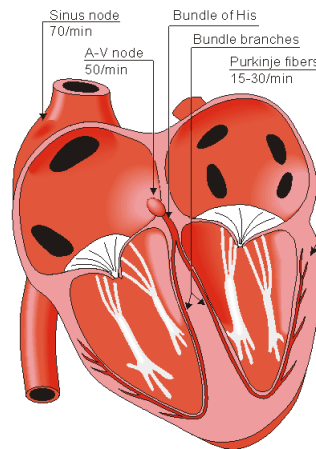
Figure 2.1: The conduction system of the heart [1].
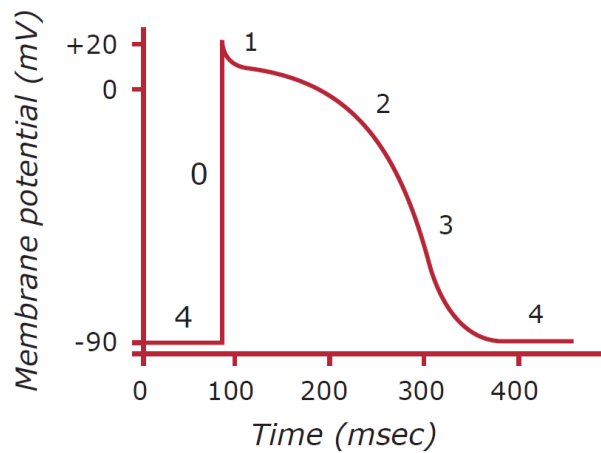
Figure 2.2: A typical action potential from a ventricular myocardial cell.

drop occurs within 2 to 3 ms to a plateau level value (caused by the closure of Na^+ channels). This is followed by plateau phase (phase 2) caused by opening of slow Ca^{2+} channels. This phase lasts for most duration of the action potential. After this, repolarization follows (phase 3), during which the action potential falls back to its resting value. This is caused by closing of Ca^{2+} channels and outflow of K^+ ions. Steady state between action potentials is phase 4 [5].

3   Heart cell modeling

At first, it may seem simple to assemble a model of heart cells, but these models must include properties whose modeling is not easy (for example, the correct conduction velocity, APD restitution, memory, and a nonzero minimum cycle length etc.). However, in order to maintain the best computational tractability is not necessary that each model contains all these features, but must be retained all the characteristics important for the particular study (action potentials calculated by various model can be seen in Figure 3.1) [6].

Models can be divided into two basic categories: entirely physiological and simplified, but the boundaries between these models, is very unclear. Detailed cellular models may contain tens to hundreds of variables and equations. In contrast, the simplified models generally contain up to ten variables and smaller number of equations [6]. It follows the basic difference between simplified and completely physiological model. While physiological models can better reproduce the properties and behavior of cardiac cells, they are more complex and therefore are unsuitable for use in demanding simulations. Meaning of the parameters in physiological model may not be entirely clear and may therefore be very difficult to find the value of these parameters.

Simplified models that are used for modeling of cardiac electrophysiology can be broadly divided into three categories: direct reduction of more detailed models, general models and phenomenological models [6].

Reduced models are created by reducing the complexity of the physiological model (for example by replacing the rapidly changing variables by their equilibria, removing slowly changing variables or reduction of variables so that they will take some (or all) of intracellular ion concentrations as constant [6].

Another type of simplified model are generic models of excitable media. An example of this model is, for example FitzHugh-Nagumo model [7] (originally the model of neuron). These models but lack important features.

The last type are phenomenological models. These types of models trying to reproduce the dynamic properties of the inclusion of a limited amount of biophysical detail. These models include model Fenton-Karma [3, 6].

Propagation of the action potential in cardiac tissue is a complex process and models that simulate that process must meet certain characteristics to describe the plot correctly.

One of these parameters is conduction velocity (CV), which is determined by several factors, including for example membrane excitability, conduction in cardiac tissue (reducing these two parameters may result in a reduction of the CV and result in a propagation block) and duration of stimulation cycle (CV restitution). At higher stimulation is usually decrease the CV, because the heart tissue is not yet fully repolarized [6].
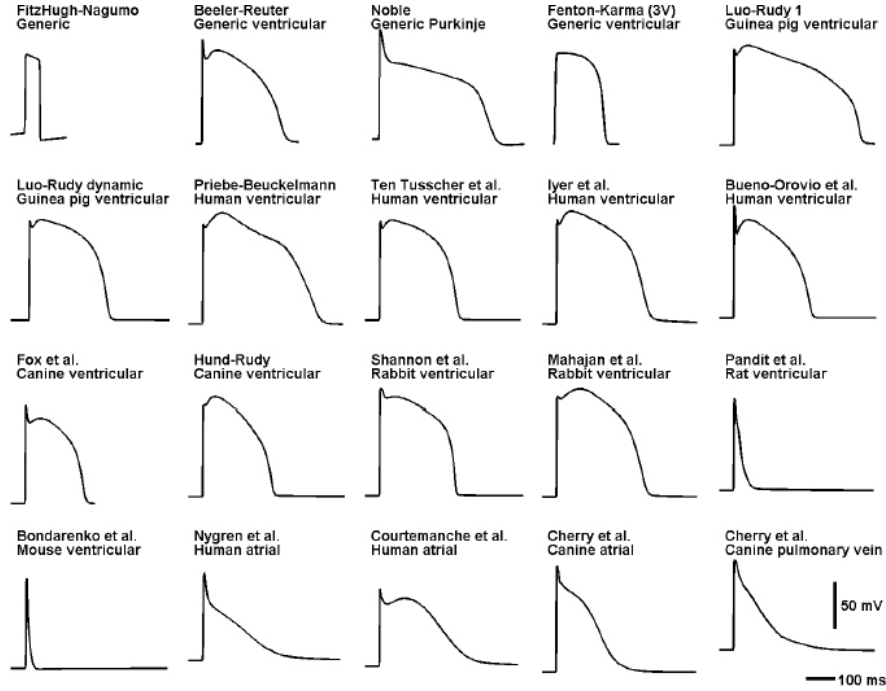
Figure 3.1: The action potentials of various mathematical models of heart cells [2]
.

Another feature of the spread of the action potential is anisotropy, which results from organizations of cardiac myocytes fibers. Propagation is thereby faster along the major axis of the muscle fiber, which leads to axisymmetric anisotropy, which is characterized by using two values CV (with fibers parallel and perpendicular to these fibers). An important factor that affects the speed of propagation of the wave is also the curvature of the action potential, where three wavefront are typical (planar, convex and concave) [6].

The anisotropy can be related to other division of models - to bidomain and monodomain. Bidomain heart tissue model takes into account the different anisotropy of extracellular and intracellular space. Monodomain model is a simplification of the model bidomain. Conductivity in the extracellular space is proportional to the intracellular compartment.

$$G_e = \lambda G_i$$

where λ is scalar indicating the proportion between spaces. Anisotropy is therefore the same in these spaces. Monodomain equation is often written as

$$\frac{\partial V_m}{\partial t} = \nabla \cdot \mathbf{D}\nabla V_m - \frac{i_{ion}}{C_m}$$

Where $\mathbf{D}$ is the diffusion tensor or scalar diffusion coefficient, V_m stands for transmembrane

voltage, i_{ion} is sum of transmembrane currents and C_m stand for capacity of the cell membrane [6].

As apparent from the above, setting the parameters of the models is very complex and a large number of studies is about a suitable method of finding the parameters. Pattern for determining the parameters are experimental data, or in the case of simplified models of propagation of the action potential is physiological model. Another option defining the parameters of the model is to create a patient-specific parameter sets. Which will reflect well the patient's cardiac electrophysiology.

Determination of the individual parameters generally difficult problem, which is engaged in numerous studies. The simplest approach is to change the parameters to achieve the targeted properties. Given that the parameters generally affect more than one property model, this approach is only possible with simple models. Usually it is required a more sophisticated approach. Determining the parameters of the heart model deals for example in [8]. The authors have collected data using electrophysiological experiments, and then using a genetic algorithm determine model parameters so that the simulation results copied the measured data.

The resulting models are then used, for example, to investigate the effects of defibrillation or, for example, to examine cardiac arrhythmias such as ventricular fibrillation and their effects on cardiac tissue.

4 FK3V model

4.1 FK3V model description

Fenton-Karma model (FK3V) is a dimensionless ionic model of cardiac action potential, which is based on the Luo-Rudy I model. For reproducing action potential it uses three variables u, v, and w. Variable u represents the transmembrane potential (so that $u = 0$ and $u = 1$ are the rest and peak voltages, respectively). Output from this model can be seen in Figure 4.2. The transmembrane potential changes depending on ionic currents according to the following equation:

$$\dot{u} = J_{stim} - J_{fi} - J_{so} - J_{si} \tag{4.1}$$

where J_{fi} (accountable for depolarization of the membrane), J_{so} (accountable for repolarization of the membrane), and J_{si} (balances J_{so} during the plateau phase) are cross-membrane currents named fast inward (fi), slow outward (so), and slow inward (si) that roughly corresponds to sodium, potassium, and calcium ion currents, respectively. But because they do not represent the quantitatively measured currents but only their activation, inactivation, and reactivation, it is preferred to call these currents as fast and slow inward, and slow outward, rather than Na, Ca, and K as a reminder of these simplification. J_{stim} indicates the externally applied current. In this study, the external current composition of pulses is created by the first half period of sine function followed by zero function. J_{stim} is therefore defined by the following equation:

$$J_{stim} = \begin{cases} A\sin(t - n(c+1)) & t \in [n(c+1), n(c+1)+1] & n \in \mathbb{N} \cup \{0\}, \\ 0 & t \notin [n(c+1), n(c+1)+1] & n \in \mathbb{N} \cup \{0\}, \end{cases} \tag{4.2}$$

where c denotes the length of time interval between pulses and A stands for the amplitude. Here $\dot{u}$ denotes the first derivative of u with respect to time. This function can be seen in Figure 4.1.

The cross membrane currents are given by

$$J_{fi}(u; v) = \Theta(u - u_c)(1 - u)(u - u_c)\frac{-v}{\tau_d},$$

$$J_{so}(u) = \Theta(u_c - u)\frac{u}{\tau_0} + \Theta(u - u_c)\frac{1}{\tau_r}, \tag{4.3}$$

$$J_{si}(u; w) = \frac{-w(1 + \tanh(k(u - u_c^{si})))}{2\tau_{si}},$$

where $\Theta(x)$ is the Heaviside function which replaced the gating functions $h_\infty(V)$, $m_\infty(V)$, $j_\infty(V)$, and $f_\infty(V)$, in the Beeler-Reuter or Luo-Rudy-I models. Function $d_\infty(V)$ is replaced by smooth
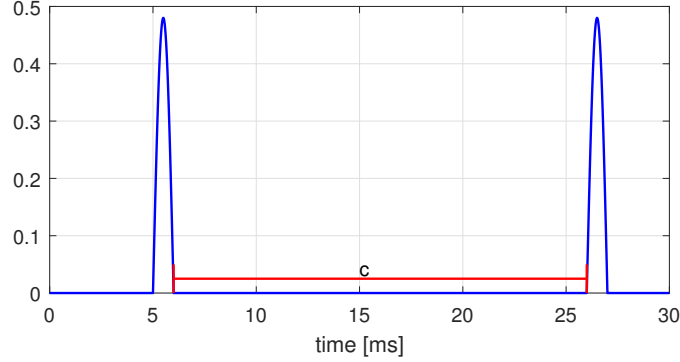
Figure 4.1: Stimulation function with labeled parameter c (red).

function

$$\frac{(1 + \tanh(k(u - u_c^{si})))}{2}$$

to provide good fit of APD restitution curves.

Another two variables v and w used in the model are gating variables which regulate inactivation of J_{fi}, and J_{so} takes the following form:

$$\dot{v} = \Theta(u_c - u)(1 - v)\frac{1}{\tau_v^-(u)} - \Theta(u - u_c)v\frac{1}{\tau_v^+}, \tag{4.4}$$

$$\dot{w} = \Theta(u_c - u)(1 - w)\frac{1}{\tau_w^-} - \Theta(u - u_c)w\frac{1}{\tau_w^+}, \tag{4.5}$$

$\tau_v(u)$ is a function for defining the time constants for two voltage ranges ($u_v < u < u_c$ and $u < u_v$) and is introduced for proper reproducing CV restitution curve. It controls reactivation of J_{fi} and is given by equation

$$\tau_v^-(u) = \Theta(u - u_v)\tau_{v_1}^- + \Theta(u_v - u)\tau_{v_2}^-$$

The model contains several constants, which are used for fitting the output curves into the requested shape, time constants τ_r, τ_{si}, τ_0, threshold potentials u_c, u_c^{si}, and u_v.

The original paper [3] describes four different sets of parameters to fit for different dataset.

- BR: obtained by stimuli of the Beeler-Reuter model with standard parameter values.

- MBR: obtained by stimuli of modified the Beeler-Reuter model with accelerated up calcium kinetic.

- MLBR-I: stimuli of Luo-Ruby-I model with speeded up calcium kinetic.
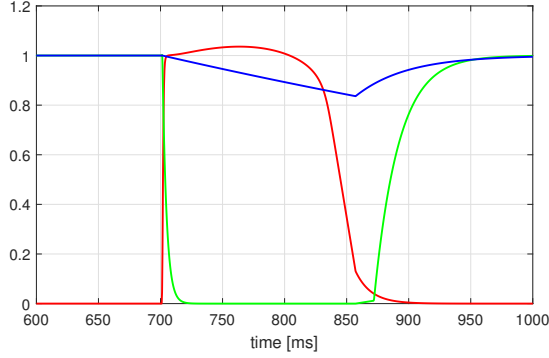
Figure 4.2: Variable u (red), v (green) and w (blue) of FK3V model with BR parameter set.

- GP: experimental data from measuring the membrane potentials on the epicardial surface of the left Ventricle of a guinea pig.

Table 4.1: Original published parameters of the FK3V model [3] for BR parametric set, $k = 10$

Parameter	Description	unit	value
τ_d	setting influence J_{fi} for $u > u_c$	ms	0.25
τ_r	setting influence J_{so} for $u > u_c$	ms	33
τ_{si}	setting influence J_{si} on $\dot{u}$	ms	30
τ_0	setting decrease u to 0 for $u < u_c$	ms	12.5
τ_v^+	setting decrease v to 0 for $u > u_c$	ms	3.33
$\tau_{v_1}^-$	setting value for $\tau_v^-(u)$ for $u > u_v$	ms	1250
$\tau_{v_2}^-$	setting value for $\tau_v^-(u)$ for $u < u_v$	ms	19.6
τ_w^+	setting decrease w to 0 for $u > u_c$	ms	870
τ_w^-	setting increase w to 1 for $u < u_c$	ms	41
u_c	depolarization threshold	-	0.13
u_v	threshold for activation $\tau_{v_1}^-$ or $\tau_{v_2}^-$	-	0.04
u_c^{si}	threshold for opening J_{si}	-	0.85

4.2 Model improvement

Since the shape of FK3V model is not realistic, the modification of this model is proposed. The modification consists of replacing constant τ_r in Equation (4.3) by the following function

$$\tau_r(u) = \Theta(u_{\tau_r} - u)\tau_r + \Theta(u - u_{\tau_r})\Big(\frac{\tau_r(1 + \tanh(k_2(1 - u)))}{4} + \frac{\tau_r}{2}\Big). \tag{4.6}$$

This equation divides $\tau_r(u)$ into two potential ranges. From 0 to u_{τ_r} where $\tau_r(u)$ remains constant and from u_{τ_r} above, where u decreases from τ_r to $\tau_r/2$. Another parameter introduced

in Equation (4.6) is k_2 which sets the speed of decrease of $\tau_r(u)$. In this work $u_{\tau_r} = 0.85$ and $k_2 = 20$. Another change from the original model is redefining u_c^{si} to value $u_c^{si} = 0.7$. The rest of the parameters stay the same as in the original BR parameters set (see Table 4.1).

In Figure 4.3, the difference in the shape of the transmembrane potential of the original FK3V model as well as the modified model can be seen.
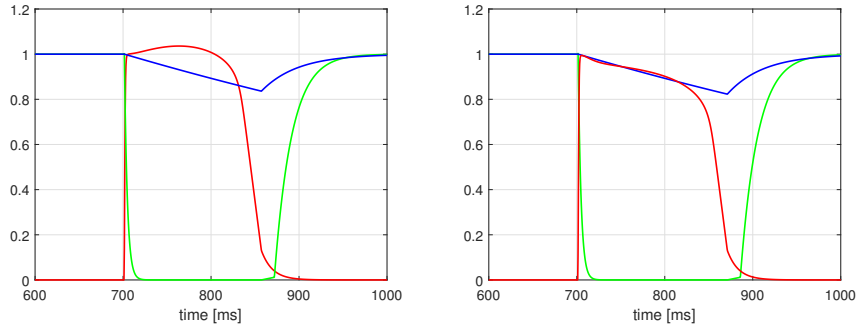
Figure 4.3: Time responses of u (red), v (green) and w (blue) of the original model (left) and improved model (right) for $c = 700$ ms and $A = 0.48$.

4.3 Using of FK3V model

FK3V model is commonly used to describe a simplified model of the heart and electrophysiology studies that use this model can be generally divided into several groups. Studies dealing with the determination of parameters of models to better replicate the outputs obtained by using physiological models and experimental data, studies that use the model to study the electrophysiology of the heart and studies that examine the characteristics of the model FK3V.

The first group can include for example the study [9], which describes a procedure for finding such parameters FK3V model to its restitution characteristics correspond restitution characteristics of Courtemanche-Ramirez Nattel model of atrial tissue. In [10], the authors then edited the parameters of detailed and simplified (FK3V) model to fit for five clinical data of patients undergoing ablation therapy. The authors focused on fitting the shape of the action potential, action potential duration, restitution and conduction velocity. Fitting was done using simulated annealing fitting procedure and the resulting model accurately reproduced the clinical data, but the parameters were significantly different from the original parameters of published authors, and also between individual patients. Both models (detailed and simplified) reproduce a similar spiral wave dynamics, which are however different for each patient.

In [11] authors carry out entrainment pacing to group of patient undergoing radiofrequency ablation of atrial and ventricular reentrant arrhythmias. This process is then simulated using 2D model of cardiac tissue using a model FK3V. The authors investigated postpacing interval

(PPI) and the tachycardia cycle length (TCL; PPI-TCL) interval to assess the reproducibility of the interval, both in vitro and in silico. The authors found a high repeatability with differences ≤ 20 ms between the results for each stimulation. In the case of slow tachycardia, parameter variability is significantly lower.

Termination of fibrillation is studied in [12]. Their objective was to numerical validation the experimental techniques for terminating fibrillation presented in [13]. As a numerical model authors used the FK3V. In his work, they found that synchronized defibrillation can create a low-energy alternative to traditional defibrillation. In [14] the authors studied electrophysiology and dynamic mechanism of spiral waves break up (which are one of the main mechanisms of fibrilation to raise). This work simulated 2D cardiac tissue with the FK3V model. The authors found several alternans unstable modes with different growth rates, frequencies and spatial structures. Instability mode is increased along with the increase of conductivity of fast inward current. The work also using eigenmode methods to calculate the exact time and amplitude of the stimulus, which was then optimally located so as to ensure maximum efficiency. The authors come to the special case where the spiral wave break up was suppressed with a single stimulus. In a study [15], the authors examined the behavior of fibers in a computing FK3V monodomain anisotropic model of re-entrant ventricular fibrillation. In [16] focused on the optimal control based on the cardiac electrophysiology bidomain equations in conjunction with FK3V. The basic tools for successful defibrillation used in this work are shape calculus and marching cubes algorithm.

Another topic which often target individual work dealing with FK3V model is descriptions of properties of the model itself. Example of this study is [17], which examines steady state of the system. Linear stability of these points and their response to external stimulation were examined.

5 Dynamical properties detection tools

In this chapter, a brief introduction to methods exploring a dynamic system properties are given. These tools will be explained and demonstrated using well known Lorenz system of ordinary differential equations (5.1) which are used for modeling atmospheric convection. It is system with three degrees of freedom (x, y and z) and three different parameters (ρ, σ and β). These equations exhibits regular as well as chaotic patterns.

Equations were solved numerically using the explicit Runge-Kutta method implemented as *ode23* solver in Matlab. Equations were solved with initial conditions $x = y = z = 1$ in timespan from 0 to 15000

$$
\begin{aligned}
\frac{dx}{dt} &= \sigma(y - x), \\
\frac{dy}{dt} &= x(\rho - z) - y, \\
\frac{dz}{dt} &= xy - \beta z.
\end{aligned}
\tag{5.1}
$$

5.1 Phase diagram

Phase space (or state space) is a notion proposed by Ludwig Boltzmann, Henri Poincaré, and Willard Gibbs in the 19th century. It is set of all the possible states of the dynamical system. A diagram, where all states are marked is phase diagram (the state of the system is represented as a point). In the phase diagram (phase portrait), every degree of freedom of the dynamical system is represented by the axis in the multidimensional space. This tool is suitable for example to distinguish between stable and chaotic behavior [18].

Example of phase diagram can be seen in Figures 5.1 and 5.2. In Figure 5.1 examples of phase diagram depicting stable orbit is given. In Figure 5.2 is shown example of chaotic attractor.

5.2 Poincaré section

Let's have a dynamical system in continuous time

$$\dot{x} = f(x)$$

where $x \in \mathbb{R}^n$. Now, in the phase space of this dynamical system, define a section with lower dimension called Poincaré section (named after Henri Poincaré). Next step is to compute all intersections of Poincaré section with state space and plot them to graph. Intersections are represented as points, and the set of all intersections is called Poincaré map. This map can be
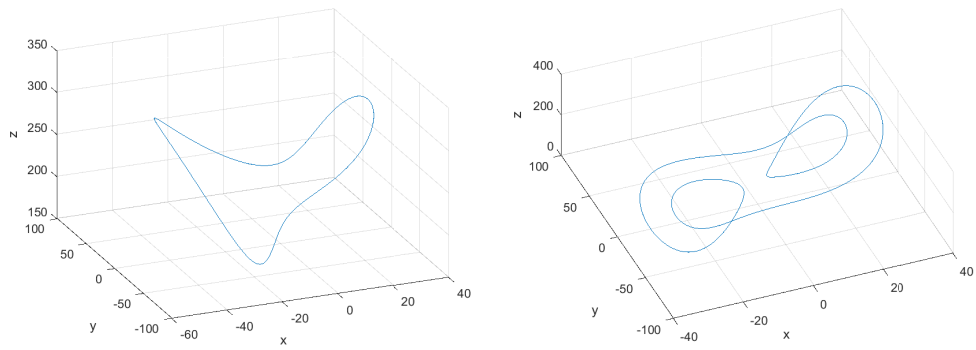
Figure 5.1: Phase diagram of stable orbit of system (5.1) with parameters $\rho = 240$, $\sigma = 10$ and $\beta = {}^8\!/\!{}_3$ (left) and parameters $\rho = 150$, $\sigma = 10$ and $\beta = {}^8\!/\!{}_3$ (right).
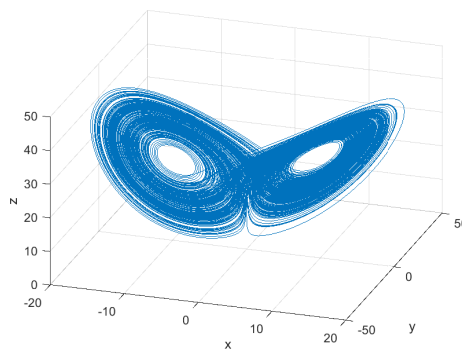
Figure 5.2: Phase diagram of Lorenz equations with parameters $\rho = 28$, $\sigma = 10$ and $\beta = {}^8\!/\!{}_3$.

Figure 5.3: Phase diagram of Lorenz equations with depicted Poincaré section parameters $\rho = 240$, $\sigma = 10$ and $\beta = {}^8\!/_3$ (left) and Poincaré map (right).

Figure 5.4: Phase diagram of Lorenz equations with depicted Poincaré section parameters $\rho = 150$, $\sigma = 10$ and $\beta = {}^8\!/_3$ (left) and Poincaré map (right).

seen as a discrete dynamical system (with less degrees of freedom than the original continuous system). This tool is often used in practice for dynamical system analysis, because it displays many properties of periodic, quasi-periodic and chaotic orbits, and dynamical system behavior is interpreted in lower dimensions. There is no general procedure for constructing the Poincaré section. The information obtained with this tool is dependent on the location of the subspace in which the intersection is calculated.

Example of Poincaré map can be seen in Figures 5.3, 5.4 and 5.5. In Figure 5.3 only one point can be seen. This illustrates stable orbit with period 1 (intersection is only in one point of Poincaré section) of Poincaré map. Another examples of stable period orbit can be seen in Figure 5.4. This Figure represents stable orbit of Poincaré map with period 2 (in the right part of Figure can be seen only two points). Example of Poincaré map created from chaotic attractor is depicted in Figure 5.5. Chaotic behavior indicates line created from intersection of Poincaré section and state space. By comparing Figures 5.4 and 5.6, dependence on Poincaré section
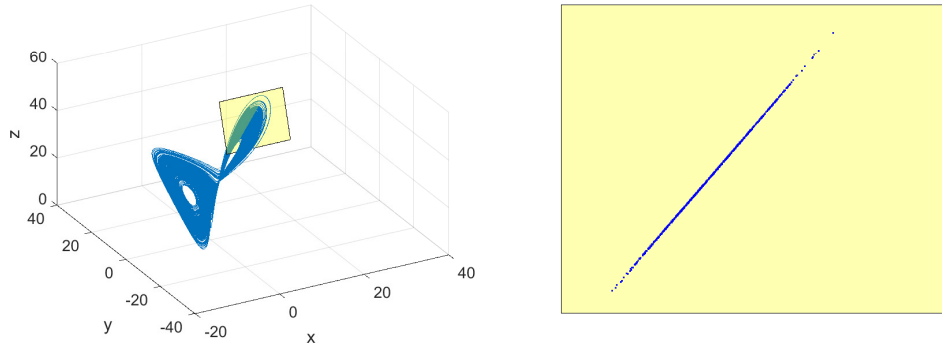
Figure 5.5: Phase diagram of Lorenz equations with depicted Poincaré section parameters $\rho = 28$, $\sigma = 10$ and $\beta = 8/3$ (left) and Poincaré map (right).
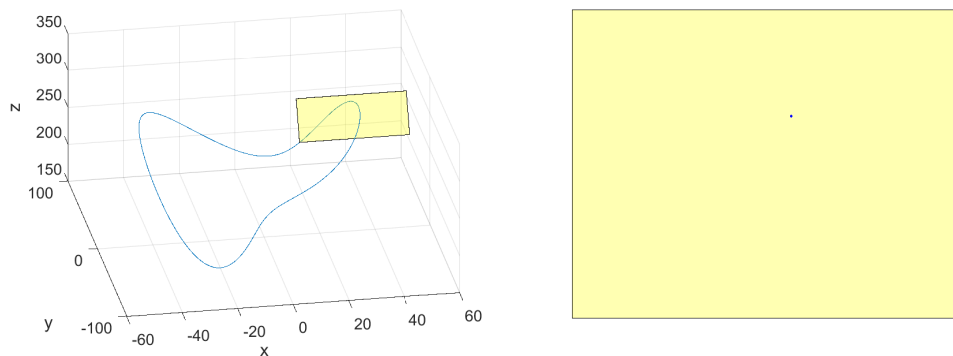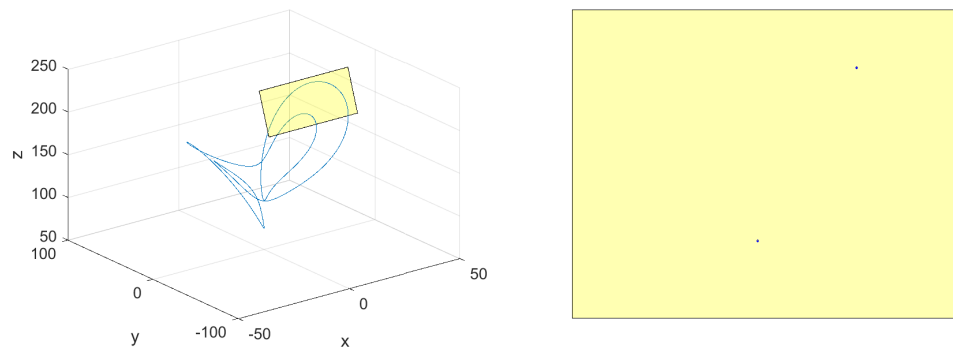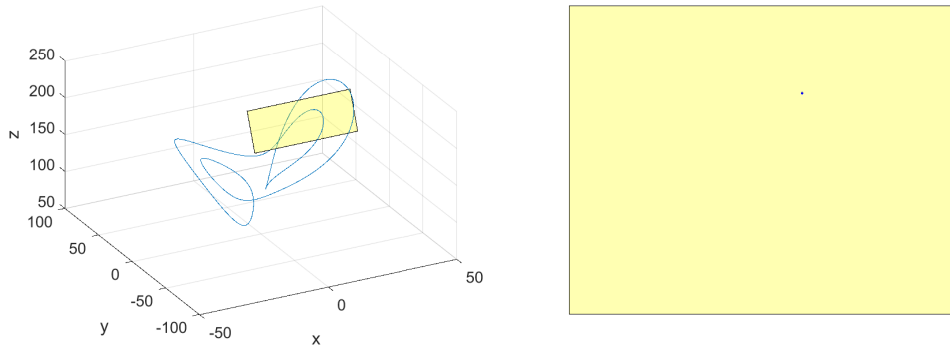

Figure 5.6: Phase diagram of Lorenz equations with depicted Poincaré section parameters $\rho = 150$, $\sigma = 10$ and $\beta = 8/3$ (left) and Poincaré map (right).

placement can be seen. While in Figure 5.4, two points depicting period 2 orbit of Poincaré map is shown. In Figure 5.6 can be seen only one point suggesting period 1 solution. This difference is caused by shifting Poincaré section to different location in phase space.

5.3 Bifurcation diagram

Let's have a dynamical system dependent on parameters. Let's write this system in continuous time as

$$\dot{x} = f(x, \alpha), \tag{5.2}$$

or in discrete time case as

$$x \mapsto f(x, \alpha), \tag{5.3}$$

where $x \in \mathbb{R}^n$ and $\alpha \in \mathbb{R}^m$ denotes phase variables and parameters, respectively. As the parameters α changes, the phase portrait of system (5.2) and (5.3) also varies. These changes

28
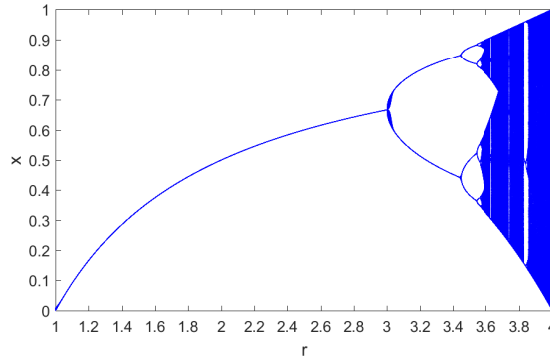
Figure 5.7: Bifurcation diagram of Logistic map with respect on parameter r and $x_0 = {}^2/_3$.

may result in two options: system stay topologically equivalent to the original one, or its topology will be different [19].

Definition 5.1 ([19]) *The appearance of a topologically nonequivalent phase portrait under variation of parameters is called a **bifurcation**.*

Bifurcation is therefore a change of the topological type of system (5.2) or (5.3) when its parameters pass through a bifurcation (critical) value [19]. To capture these changes, a bifurcation diagram is usually created. It is a graphical representation of the relationship between bifurcation parameter and behavior of the system. In this diagram, system behavior (fixed points, periodic orbits, or chaotic attractors etc.) can be distinguished.

Definition 5.2 ([19]) *A **bifurcation diagram** of the dynamical system is a stratification of its parameter space induced by the topological equivalence, together with representative phase portraits for each stratum.*

In order to maintain the greatest possible clarity, the bifurcation diagram will be presented on Logistic map (5.4).

$$x_{n+1} = rx_n(1 - x_n) \tag{5.4}$$

Bifurcation diagram of Logistic map is depicted in Figure 5.7. In this diagram can be seen period 1 solution (fixed point) for parameter $1 \leq r \leq 3$ as only one point for $1 \leq r \leq 3$ can be seen. In $r = 3$ bifurcation occurs and solution with period 2 can be found for $3 \leq r \leq 3.44949$. After that, another bifurcation appears and period 4 solution can be found. This phenomena called *period doubling* continuous until $r = 3.5699456$ where chaotic behavior of Logistic map starts and bifurcation diagram shows line which implies non-periodic motion. Another stable solution of period 3 can be found at interval $3.831874055 \leq r \leq 3.857082826$.
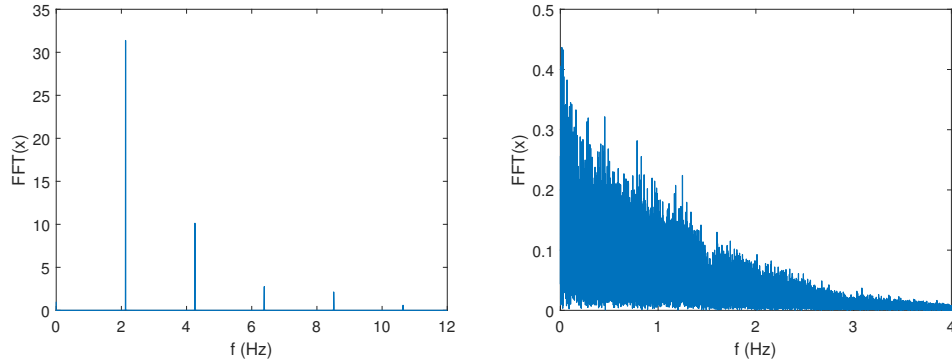
Figure 5.8: Fourier spectra of (5.1) with parameters $\rho = 240$, $\sigma = 10$ and $\beta = {}^8\!/_3$ (left) and parameters $\rho = 28$, $\sigma = 10$ and $\beta = {}^8\!/_3$ (right).

5.4 Fourier spectra

This is a very popular tool, since the idea of decomposing a non-periodic signal into a set of sinusoidal or harmonic signals is well known. This method is based on the assumption that combination of the sine or cosine signals can represents a periodic or non-periodic signal:

$$f(t) = \frac{1}{2\pi} \int_\Gamma F(\omega) e^{i\omega t} d\omega$$

Since $F(\omega)$ is in many cases complex, for graphical representation the absolute value $|F(\omega)|$ is used [20].

In case of periodic, or quasi-periodic motion, graphical representation of Fourier spectra shows narrow peaks or lines, which means, that the signal is possible to reconstruct with discrete set of harmonic functions $\{e^{\pm i\omega_k t}\}$, where $k = 1, 2, ...$ In case of chaos onset, graph depicting $|F(\omega)|$ with continuous frequencies distribution emerge. When the motion is in fully chaotic regime is possible that in continuous spectrum dominates the discrete spikes [20].

Differences in Fourier spectra between these two motions are represented in Figure 5.8. In Figure 5.8 (left), Fourier spectrum of stable behavior is shown. Peaks in this graph represents discrete set of harmonic functions. In Figure 5.8 (right), continuous frequency spectrum of chaotic motion is depicted. Here, the Fourier spectra is formed by a number of harmonic components having the basic, super-harmonic, sub-harmonic, and combination frequencies on which there are superposed further motions with frequencies forming the sided bands of the dominant frequencies. Their mutual ratio indicates the irregularity of the motion.

6   The 0-1 test for chaos

Generally, a dynamic system can be viewed as a model of the action of a time flow T on a state space X whose elements are all possible states of the system. There are several ways to describe this system in a mathematical way. One of the options is the description using differential equations. However, since it can be seen as a dynamic system also human heart, when its activity is examined over time. Differential equations therefore can be used to describe the activity of the heart and examine this activity with tools designed for dynamic system analysis. [21]

One of the tools for analyzing dynamical systems is the 0-1 test for chaos [22, 23]. This test is used to distinguish regular and chaotic dynamics. The resulting value of this test can only be 0 (regular behavior) or 1 (chaos). This method is based on the statistical properties of a single coordinate only. Systems dynamics is then quantified by a single parameter calculated in the time domain.

Advantage of this test over the approaches based on frequency spectrum is that in this method only one parameter provides information about systems dynamics (likewise maximal Lyapunov exponent). Compared to Lyapunov exponents, however, this method is far more suited for practical applications, since it does not require linearization of the system (which is often non-trivial and sometimes difficult to achieve), but the theory behind this method is based on the long-term behavior of suitable extensions of the system with respect to the two-dimensional Euclidean group [21].

0-1 test can also be used for measured data, where the presence of noise can not be avoided (how to deal with noisy data is described for example in [23, 24]). In study [25] authors applied the 0–1 test to stochastic time series and they discovered, that pairing this with a test for determinism can be used to distinguish between chaos and randomness from a noisy data. Application of the 0-1 test for chaos to experimental data is described in [25]. In this article is taken as example data measured from electromagnetic bipolar motors. In application is also important to take into account sampling period and its possible influence to test results. There were proposed several approaches how to optimize sampling frequency and also reduce the number of elements in time series. The main thought of this approaches is to relate sampling frequency with characteristic period present in the time serie (for more details see e.g. [23]).

As it was written before, the 0-1 test for chaos is based on the exploration of the long-term behavior of the underlying dynamical system extension with respect to the two-dimensional Euclidean group (for more information about Euclidean extensions of dynamical systems see [26]). If we extend dynamical system, then in the (p, q)-plane defined using equation (6.2) is its asymptotic dynamics bounded for regular motions and unbounded for nonregular motions.

Due to computation load is this criterion in the applications applied to the projections of the trajectory on the p or the q axis (time series is therefore further simplified due to focusing only on one component of the 'virtual point') [21].

According to the statement, that occurrence of chaos is shown by unbounded motion in (p, q)-plane. In the implementation we have to choose between two ingredients which will affect the subsequent implementation of the method.

- Computation of scalar quantities from the knowledge of the trajectory. Asymptotic growth rate of this sequence can be correlated with the unboundedness.

- The way of defining the asymptotic growth rate.

In numerical tests are shown [22], that chaotic dynamical system in (p, q)-plane slant to motion with irregular behavior which is similar to Brownian motions. Probability distribution for these type of motion is Gaussian with mean x_0 and variance σ^2 which linearly increasing with time t and because Brownian motion is a ergodic process, therefore variance of these distribution is equal to the time-averaged mean-square displacement (MSD) of any specific trajectory evaluated over some time lag. Due to this, the boundedness or unboundedness of a trajectory can be determined by examining the asymptotic growth rate of MSD as a function of the time lag defined using equation (6.3) [21].

It is obvious, that displacement over the same time lag may not be the same in different parts of trajectory, therefore quantity $M_b(n)$ is average of displacements calculated during *all* time lags of duration n along the trajectory [21].

It is also appropriate to note that MSD is related to the partial power spectrum sum (for definition see [27, 28]), that can be viewed as ancestor of the 0–1 test. Therefore it can be said that MSD is scaled according to the power law.

$$MSD \sim t^{\lambda(b)}$$

where $\lambda(b)$ is the Lyapunov exponent of the spectrum at frequency b (for more details see [27]) [21].

From the knowledge of auxiliary trajectory can be calculated family of quantities parameterized by the time lag n using equation (6.3).

For the fixed value of time lag n, MSD provides knowledge about local behavior in the (p, q)-plane (local because it takes account displacement after n units of time). As the n growth, behavior of $M(n)$ yields information about eventual unboundedness of the trajectory. In case that auxiliary trajectory is bounded, resulting function $M(n)$ will be bounded. In case of linear growth of this function, the trajectory behaves like a Brownian motion [21].

Last think is defining way to describe asymptotic growth rate. In the first paper dedicated to this test, authors use average logarithmic growth rate of the MSD.

$$K_b := \lim_{n \to \infty} \frac{\log M(n)}{\log n} \tag{6.1}$$

In paper [26] is shown, that in chaotic case, the dynamics of this extension is unbounded but sublinear. That's why there are two possibilities, $K_b = 0$ for a regular motion or $K_b = 1$ for a chaotic trajectory. Therefore K_b is natural indicator for the presence of chaos. It is important to note, value calculated using equation (6.1) is dependent on the parameter b, used for characterization of proposed Euclidean extension. Therefore parameter K_b must be calculated for several values of b and as the final value a median of these values should be taken [21].

The resulting indicator provides a knowledge, that is equivalent to the maximum Lyapunov exponent, but, by far, much easier to implement, with approach which is independent on the nature of the underlying system [21].

Equations (6.1) and (6.3) are not only one possible way of how to compute these parameters. In some cases, is even more appropriate to use some modifications of these formulas. For example, of possible modifications see e.g. papers [23, 24, 29] [21].

At last, let's complete the whole process of calculating the 0-1 test for chaos. This correlation method works as follows. For a given set of observations $\phi(j)$ for $j \in \{1, 2, \ldots, N\}$ are computed translation variables for suitable choice of $b \in (0, 2\pi)$:

$$
\begin{aligned}
p_b(n) &= \sum_{j=1}^{N} \phi(j) \cos(jb) = 1, \\
q_b(n) &= \sum_{j=1}^{N} \phi(j) \sin(jb) = 1
\end{aligned}
\tag{6.2}
$$

then the mean square displacement is computed using the following equation

$$M_b(n) = \lim_{N \to \infty} \frac{1}{N} \sum_{j=1}^{N} [p_b(j+n) - p_b(j)]^2 + [q_b(j+n) - q_b(j)]^2 \tag{6.3}$$

here $n \leq n_{cut}$ where $n_{cut} \ll N$. Then, the estimate of the modified mean square displacement is computed using the next equation

$$D_b(n) = M_b(n) - \left(\lim_{N \to \infty} \frac{1}{N} \sum_{j=1}^{N} \phi(j) \right)^2 \frac{1 - \cos(nb)}{1 - \cos(b)}.$$

Finally, the output of the 0-1 test is obtained as correlation coefficient of ξ and Δ for fixed

parameter b

$$K_b = \text{corr}(\xi, \Delta)$$

where $\xi = (1, 2, \ldots, n_{cut})$ and $\Delta = (D_b(1), D_b(2), \ldots, D_b(n_{cut}))$. Hence, K_b is dependent on the choice of b. To get K as the output of the 0-1 test, as limiting value of all K_b, the result value is taken as

$$K = \text{median}(K_b).$$

7 Main results

In individual simulations, the heart cell was stimulated with the half-sine shaped current pulses with an amplitude from $A = 0.16$ to $A = 0.96$ with step of 0.04 and duration 1 ms. The individual stimulation pulses were separated by the delay c (see Equation (4.2)). The computations were performed for the stimulation delays from 10 to 300 ms with step of 5 ms. Each simulation was done for the time from 0 to 5×10^5 ms. From the results, a phase diagram, amplitude frequency spectrum, and Poincaré section for each simulated frequency was computed. From the data was also created bifurcation diagram for the entire simulated frequency spectrum and the 0-1 test for chaos was computed.

This section is based on results that are accepted for publication in *Mathematical Methods in the Applied Sciences*, the paper is enclosed as Appendix of this thesis.

7.1 Phase portraits, the Fourier spectra, and Poincaré section

The Fourier spectra and phase portraits were computed for $A = 0.48$ (twice as needed to cause stimulation). Chaotic behavior of the model was observed on stimulation delays ranging from 30 to 50 ms and 105 ms. Regular behavior was observed elsewhere.

Cases with regular behavior can be divided into five groups (**RG1** – **RG5**). Each of these groups corresponds to the different biological response of the cell to the stimulatory pulses and corresponding representatives are shown in (Figure 7.1 – Figure 7.5); in all of these cases the Fourier spectra is formed by a number of harmonic frequencies, hence the frequency of the periodic trajectory is computable. Periodic motions of trajectories are also visible in Poincaré sections.

The irregular (chaotic) case is shown in Figure 7.6, the **IRG** case. In this case, the Fourier spectra is formed by a number of harmonic components having the basic, super-harmonic, sub-harmonic, and combination frequencies on which there are superposed further motions with frequencies forming the sided bands of the dominant frequencies. Their mutual ratio indicates the irregularity of the motion. The character of this motion's case is underlined by the Poincaré section.

RG1 This case is represented in Figure 7.1 for stimulation delay 20 ms. The amplitude of u does not reach the full range (0 to 1), but changes only between 0 and 0.34. The action potential shape (variable u) also does not match with proper shape of action potential (see Figure 4.3 for comparsion).

RG2 At stimulation delays from 75 ms to 100 ms, stimulation causes every third stimulus (two unsuccessful stimulation followed by successful pacing). In the phase diagram, a closed

Figure 7.1: From the left: time responses of u (red), v (green), and w (blue); FFT of variable u; phase diagram and Poincaré section of the modified FK3V model for $c = 20$ ms.
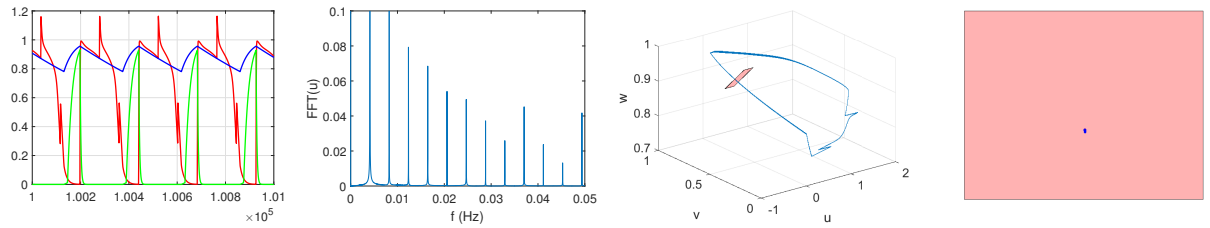
Figure 7.2: From the left: time responses of u (red), v (green), and w (blue); FFT of variable u; phase diagram and Poincaré section of the modified FK3V model for $c = 80$ ms.

loop with two spikes due to unsuccessful stimulation can be seen. The representative case of the model with this behavior can be seen in Figure 7.2.

RG3 In Figure 7.3, the typical model response for the delays ranging from 110 ms to 145 ms can be seen. The relevant stimulation is caused by every second stimulation impulse, but every second successful stimulation comes to phase of relative refracterity, therefore the action potential of this stimulation has shorter duration than the action potential of the previous successful stimulation impulse. In the phase portrait, two spikes from unsuccessful stimulation and two curves from the stimulation (one comes from the phase of relative refracterity and one comes from steady state) can be seen.

Figure 7.3: From the left: time responses of u (red), v (green), and w (blue); FFT of variable u; phase diagram and Poincaré section of the modified FK3V model for $c = 120$ ms.

Figure 7.4: From the left: time responses of u (red), v (green), and w (blue); FFT of variable u; phase diagram and Poincaré section of the modified FK3V model for $c = 160$ ms.
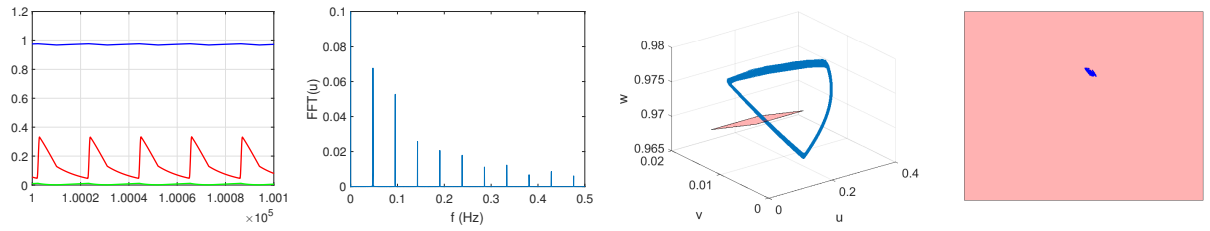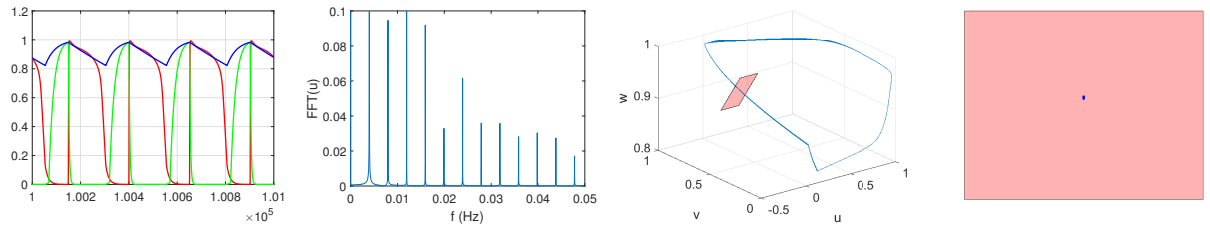

Figure 7.5: From the left: time responses of u (red), v (green), and w (blue); FFT of variable u; phase diagram and Poincaré section of the modified FK3V model for $c = 250$ ms.

RG4 In Figure 7.4, the representative case, every second stimulation impulse causes stimulation at delays from 150 ms to 185 ms. The action potential duration is about 200 ms.

RG5 Finally, in Figure 7.5, the representative is shown where every stimulation impulse causes stimulation. This is observable for delays from 190 ms and above.

IRG The behavior of motions observed on delays from 30 ms to 50 ms and 105 ms is irregular, the representative can be seen in Figure 7.6. In this case, the mutual ratio of stimulation impulse and stimulation indicates the irregularity of the motion. Moreover, these cases are chaotic due to the output of the 0-1 test for chaos performed in Section 7.3.
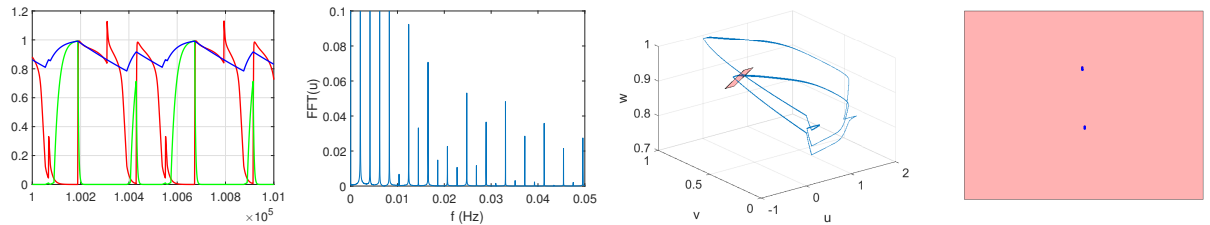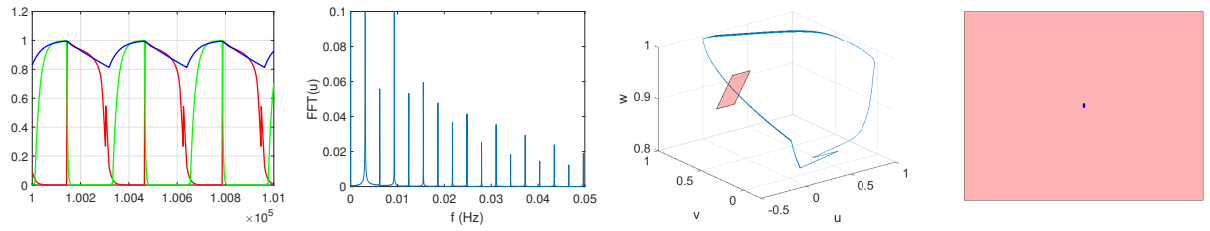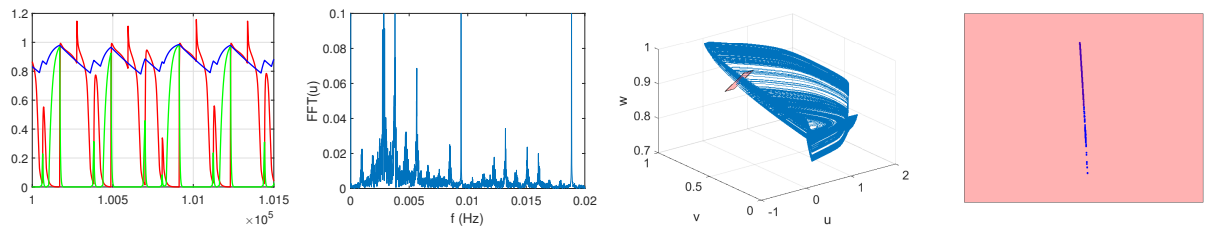

Figure 7.6: From the left: time responses of u (red), v (green), and w (blue); FFT of variable u; phase diagram and Poincaré section the modified FK3V model for $c = 105$ ms.
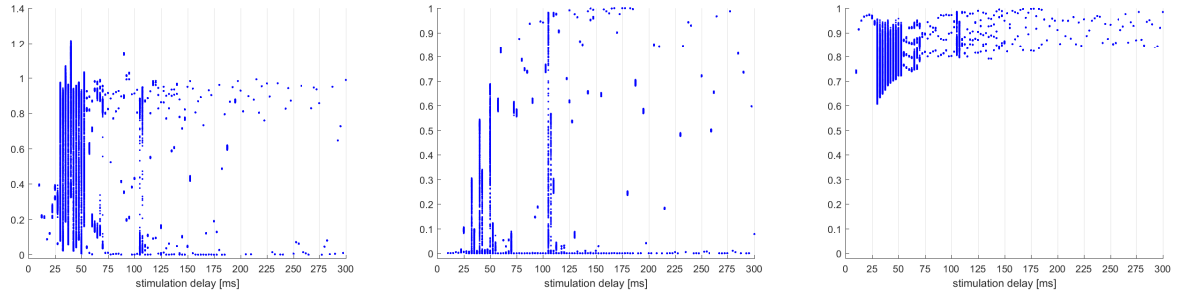
Figure 7.7: Bifurcation diagram for variable u (left), v (middle), and w (right).
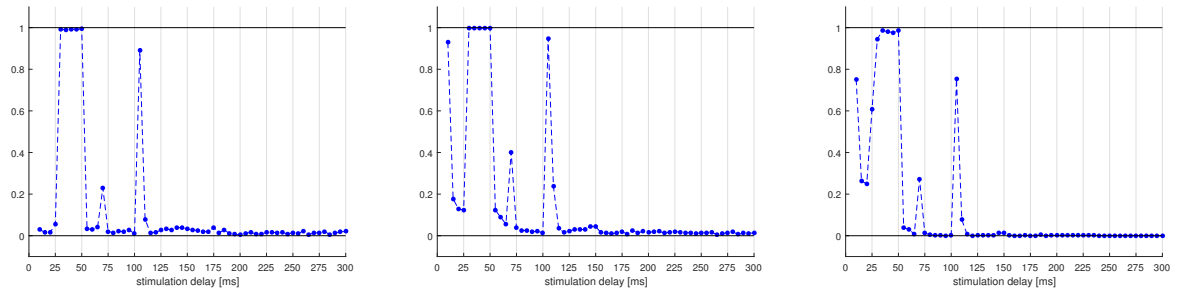
Figure 7.8: Results of the 0-1 test for chaos for $A = 0.48$ and c from 10 ms to 300 ms. Variable u (left), v (middle) and w (right).

7.2 Bifurcation diagram

Next work was to plot bifurcation diagrams of modified FK3V model. Values for diagrams was collected witch period of stimulation frequency. Diagrams can be seen in Figure 7.7. In diagrams can be seen, that stimulation delays from 30 to 50 ms and 105 ms are chaotic, at the other delays are regular responses. This coincides with time series exploration.

7.3 The 0-1 test for chaos

Next, the 0-1 test for chaos was performed. Description of this test is given in the section 7.3. The results of this test can bee seen in Figure 7.8. At delays up to 25 ms, the behavior of variable u is regular, but for variables v and w, it cannot be decided if the behavior is chaotic or regular. Chaotic behavior of the model was observed on stimulation delays from 30 to 50 ms and 105 ms. There are also several cases of stimulation delays with the output of the 0-1 test for chaos in the range $(0.1, 0.9)$; in this cases it cannot be decided if it is chaotic or regular behavior, e.g. at the stimulation delay of 70 ms. Notice, that results of this test coincides with time series and bifurcation diagram.
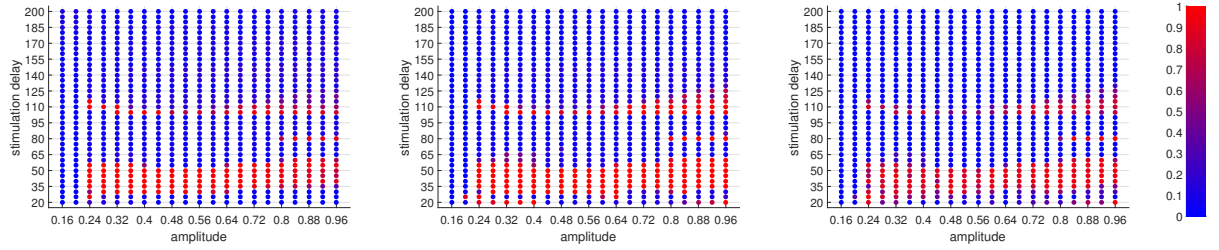
Figure 7.9: Results of the test for chaos 0-1 for various stimulation delays and amplitudes for variable (from the left) u, v, w and color bar (right).

But because of that, the stimulation of heart cell is dependent not only on the stimulation frequency but also on the amplitude of stimulation, the test for chaos 0-1 was computed also for the amplitude range from 0.16 to 0.96 in step 0.04. But since the results of the test for chaos 0-1 for $A = 0.48$ was the regular behavior for $c > 105$ ms (see Figure 7.8), the tests were computed for the stimulation delays from $c = 20$ ms to $c = 200$ ms in 5 ms increments. The results of this test can be seen in Figure 7.9. From this figure can be seen that chaotic behavior is focused into three regions.

The first and biggest region of the chaotic behavior is at amplitudes from 0.24 above and stimulation delays from approximately 30 ms to 55 ms. Another area of section of chaotic behavior is at amplitudes from 0.8 and above and stimulation delay 80 ms. And the last region of chaotic behavior is at stimulation delay around $c = 105$ ms and amplitudes from $A = 0.24$.

8 Matlab codes

In this section, the main parts of programs are provided, that were used for calculation of above mentioned results.

8.1 FK3V cardiac cell model

The code given in Listing 8.1 is for calculation of FK3V model. On the lines 1 to 26 is initialization of model parameters. On the lines 32 to 45 definition of model's functions can be seen.

```matlab
1  % model parameters (original Beeler-Reuter parameter set)
2  uc = 0.13;           % [-]
3  tauv_plus = 3.33;    % [ms]
4  tauw_minus = 41;     % [ms]
5  tauw_plus = 870;     % [ms]
6  taud = 0.25;         % Cm/gfi
7  tau0 = 12.5;         % [ms]
8  taur = 33;           % [ms]
9  k1 = 10;             % [-]
10 tausi = 30;          % [ms]
11 uv = 0.04;           % [-]
12 tauv1_minus = 1250;  % [ms]
13 tauv2_minus = 19.6;  % [ms]
14
15 % model parameters (parameters for modified model)
16 ucsi_mod = 0.7;      % [-]
17 k2 = 20;             % [-]
18 u_taur = 0.85;       % [-]
19
20 % stimulation impulse parameters
21 amp = .48;           % stimulation amplitude
22 n = 1;               % nb of pulses during one stimulation
23 a = 0;               % time to first stimuli
24 c = 105;             % time between stimulation
25 i = 1000000000;      % number of stimulation
26 T = 1;               % period of stimulatin impulse
27
```

```
28  % ode solver parameters
29  timeSpan = [0 5000];
30  opts = odeset('MaxStep',T/3); % maximum step for ode solver
31
32  % definition of function tauv_minus(u_t) (original model)
33  tauv_minus=@(y) heaviside(y(1)-uv)*tauv1_minus+heaviside(uv-y(1))*tauv2_minus;
34
35  % definition of taur modification (modified model)
36  tau_r = @(y) heaviside(u_taur-y(1))*(taur)+heaviside(y(1)-u_taur)*((taur/2)
        *((1+tanh(k2*(1-y(1))))/2)+taur/2);
37
38  % definition of modified FK3V model
39  FK3V_mod = @(t, y) ...
40     [-((-y(2)/taud)*heaviside(y(1)-uc)*(1-y(1))*(y(1)-uc)) ... % -Jfi
41     - ((y(1)/tau0)*heaviside(uc-y(1)) + heaviside(y(1)-uc)/tau_r(y)) ... %-Jso
42     - ((-y(3)/(2*tausi))*(1+tanh(k1*(y(1)-ucsi_mod)))) ...   % -Jsi
43     + (stimImp(t(1), amp, n, a, c , i, T)); ... % stimulation impulse
44     (heaviside(uc-y(1))*((1-y(2))/tauv_minus(y(1))) - heaviside(y(1)-uc)*(y(2)/
          tauv_plus)); ... % dv
45     (heaviside(uc-y(1))*((1-y(3))/tauw_minus) - heaviside(y(1)-uc)*(y(3)/
          tauw_plus))]; % dw
46
47  % solve modified FK3V model using explicit Runge-Kutta with initial conditions
        U = 0, V = 1, W = 1
48  [time, results] = ode45(FK3V_mod, timeSpan, [0 1 1], opts);
```

Listing 8.1: Matlab code for modeling transmembrane potential using modified FK3V model.

8.2 Stimulation impulse

The Listing 8.2 is used for calculation of stimulation impulse amplitude. This function is used in model definition in code 8.1 on the line 43. In this code, it is gradually decided whether a stimulus pulse is to be applied.

```
1  function y = stimImp(t, amp, n, a, c , i, T)
2  % y     output (stimulation impulse)
3  % t     time
4  % amp   stimulation impulse amplitude
```

```matlab
5   % n      nb of pulses during one stimulation
6   % a      time to first stimulus
7   % c      time between stimulation
8   % i      number of stimulation
9   % T      period of stimulatin impulse
10
11  f = 1/(2*T);    % calculate frequency of stimulus sine pulse
12  b = n*T;        % total time of stimulation
13  t1 = t - a;     % remove time to first stimulus
14  if t1 < 0       % if should not been applied yet
15      y = 0;
16  else
17      k = t1/(b+c);   % calculate the number of impulses already given
18      k1 = floor(k);
19      if k1+1 > i     % if total number of stimulation impulses has been reached
20          y = 0;
21      else
22          t2 = t1-k1*(b+c); % remove time of already given impulses
23          if t2 <= b        % if stimulation impulse should be applied
24              t3 = t-t2;    % calculate the start time of the pulse application
25              t4 = t - t3;  % calculate how long the impulse is already given
26              y = amp*sin(2*pi*f*t4); % calculate impulse amplitude
27          else
28              y = 0;
29          end
30      end
31  end
```

Listing 8.2: Matlab code for calculating stimulation impulse.

8.3   Poincaré section

The code in Listing 8.3 is used for calculation of Poincaré section. In the code, the plane, in which Poincaré section is calculated, is defined by the parametric expression (lines 7 to 19). In lines 21 to 30 are selected values, that are near to desired section. In the rest of the program are from the obtained data computed exact points in which Poincaré section intersects data obtained from code 8.1. These points are calculated using cubic spline interpolation.

```matlab
1  %% load data
2  freq;
3  data_u;
4  data_v;
5  data_w;
6
7  % define plane
8  vec_u = [1 0 0]; vec_u = vec_u/norm(vec_u);
9  vec_v = [0 -0.7 0.3]; vec_v = vec_v/norm(vec_v);
10
11 % pro c = 40:300
12 A = [0.0077 0.6523 0.9206];
13 t = [-0.1 0.1];
14 s = [-0.1 0.1];
15
16 % pro c = 20
17 % A = [0.0077+0.1, 0.6523-0.64, 0.9206+0.05]; % pro c = 20
18 % t = [-0.1 0.05];
19 % s = [-0.0 0.01];
20
21 prunik = [];
22 prec = 10^(-4);
23 for a = 1:length(data_u)
24     s1 = (data_v(a)-A(2)-((data_u(a)*vec_u(2))/vec_u(1))-((A(1)*vec_u(2))/vec_u
           (1)))/(vec_v(2)-(vec_v(1)*vec_u(2))/vec_u(1));
25     t1 = (data_u(a)-A(1)-s1*vec_v(1))/vec_u(1);
26     z1 = A(3)+t1*vec_u(3)+s1*vec_v(3);
27     if data_w(a)>=(z1-prec) && data_w(a)<=(z1+prec) && s1>=min(s) && s1<=max(s)
            && t1>=min(t) && t1<=max(t)
28         prunik = [prunik a];
29     end
30 end
31
32 start = prunik(1);
33 spline_data_x = [];
34 spline_data_y = [];
```

```matlab
35  spline_data_z = [];
36  for a = 2:length(prunik);
37      if (prunik(a)-prunik(a-1)) > 1
38          stop = prunik(a-1);
39
40          if stop - start > 1
41          vector_u = (data_u(start)+data_u(stop))/2;
42          vector_v = (data_v(start)+data_v(stop))/2;
43
44          s11 = (vector_v-A(2)-((vector_u*vec_u(2))/vec_u(1))-((A(1)*vec_u(2))/
                  vec_u(1)))/(vec_v(2)-(vec_v(1)*vec_u(2))/vec_u(1));
45          t11 = (vector_u-A(1)-s11*vec_v(1))/vec_u(1);
46          value = A(3)+t11*vec_u(3)+s11*vec_v(3);
47          spline_data_z = [spline_data_z, value];
48
49          dataIndex = spline(data_w(start:stop),start:stop,value);
50          spline_data_x = [spline_data_x, spline(start:stop,data_u(start:stop),
                  dataIndex)];
51          spline_data_y = [spline_data_y, spline(start:stop,data_v(start:stop),
                  dataIndex)];
52          end
53
54          start = prunik(a);
55      end
56      if a == length(prunik)
57          stop = prunik(end);
58
59          if stop - start > 1
60          vector_u = (data_u(start)+data_u(stop))/2;
61          vector_v = (data_v(start)+data_v(stop))/2;
62
63          s11 = (vector_v-A(2)-((vector_u*vec_u(2))/vec_u(1))-((A(1)*vec_u(2))/
                  vec_u(1)))/(vec_v(2)-(vec_v(1)*vec_u(2))/vec_u(1));
64          t11 = (vector_u-A(1)-s11*vec_v(1))/vec_u(1);
65          value = A(3)+t11*vec_u(3)+s11*vec_v(3);
66          spline_data_z = [spline_data_z, value];
67
```

```
68          dataIndex = spline(data_w(start:stop),start:stop,value);
69          spline_data_x = [spline_data_x, spline(start:stop,data_u(start:stop),
                dataIndex)];
70          spline_data_y = [spline_data_y, spline(start:stop,data_v(start:stop),
                dataIndex)];
71      end
72
73    end
74 end
```

Listing 8.3: Matlab code for Poincaré section.

8.4 Bifurcation diagram

In Listing 8.4 can be seen code for calculation bifurcation diagram from results obtained using code 8.1. Values for diagram are plotted with frequency equal to stimulation frequency. Therefore for bigger stimulation frequency, more data points are plotted. At first, parameters of bifurcation diagram are sets (lines 1 to 7). On the line 8 to 15, maximum plotted data points per stimulation delay is find out and matrices for saving the results are allocated. Lines 22 to 28 loads simulated results. On the lines 30 to 39 is calculated frequency of stimulation and at these times the data for plotting are selected. In the end are data saved to matrix.

```
1  % parameters
2  n = 1;
3  lowestTimeStep; % time step in data
4  frequency; % frequencies to plot
5  frq = min(frequency);
6  maximumTimeStart; % start of simulation
7
8  % Find out how much data will be needed for bifurcation diagram
9  time; % load time
10 time2plot = maximumTimeStart:(frq+1)*n:max(time); % times to plot
11 resIndex2plot = round(time2plot*(1/lowestTimeStep)-(maximumTimeStart*(1/
      lowestTimeStep))+1); % indexes times to plot
12
13 bifDiagram_matrix_u = ones(nbOfFrequencies, length(resIndex2plot))*(-100);
14 bifDiagram_matrix_v = ones(nbOfFrequencies, length(resIndex2plot))*(-100);
15 bifDiagram_matrix_w = ones(nbOfFrequencies, length(resIndex2plot))*(-100);
```

```matlab
16
17  index = 1;
18  for frq = frequency
19
20      display(frq); disp('bifurcation diagram');
21
22      nameRes_u = [ 'FKmodification_interp',num2str(frq),'_u.mat' ];
23      nameRes_v = [ 'FKmodification_interp',num2str(frq),'_v.mat' ];
24      nameRes_w = [ 'FKmodification_interp',num2str(frq),'_w.mat' ];
25
26      load(nameRes_u,'interpPoints_u'); % load result data
27      load(nameRes_v,'interpPoints_v'); % load result data
28      load(nameRes_w,'interpPoints_w'); % load result data
29
30      % times to plot
31      time2plot = maximumTimeStart:(frq+1)*n:max(time);
32
33      % indexes times to plot
34      resIndex2plot = round(time2plot*(1/lowestTimeStep)-(maximumTimeStart*(1/
            lowestTimeStep))+1);
35
36      % data for plotting
37      output2plot_u = interpPoints_u(resIndex2plot);
38      output2plot_v = interpPoints_v(resIndex2plot);
39      output2plot_w = interpPoints_w(resIndex2plot);
40
41      % save to matrix
42      bifDiagram_matrix_u(index, 1:length(output2plot_u)) = output2plot_u;
43      bifDiagram_matrix_v(index, 1:length(output2plot_v)) = output2plot_v;
44      bifDiagram_matrix_w(index, 1:length(output2plot_w)) = output2plot_w;
45
46      index = index + 1;
47  end
```

Listing 8.4: Matlab code for plot bifurcation diagram.

8.5 The 0-1 test for chaos

The 0-1 test for chaos is calculated in Listing 8.5. At first, parameters for test calculation are sets (lines 1 to 13). Then, the average value of tested data is calculated (line 15 to 18). After that, translation variables are computed. On the lines 41 to 54, the mean square displacement and the estimate of the modified mean square displacement is computed. At the end (line 57), correlation coefficient is calculated.

```matlab
1   % load data
2   res; % loaded data
3   skip=100;
4
5   RS=size(res);
6   n1=1;
7   n2=RS(1);
8
9   phi=res(n1:skip:n2,3);
10  phi=phi';
11  N=size(phi,2);
12
13  ncut=floor(N/10);
14
15  Ephi=0;
16  for j=1:1:N
17      Ephi=Ephi+(1/N)*phi(j);
18  end
19
20  Kc=zeros(310,1);
21  for m=1:1:310
22      c=m/100;
23
24      pc=zeros(N,1);
25      qc=zeros(N,1);
26
27      pc(1)=phi(1)*cos(c);
28      qc(1)=phi(1)*sin(c);
29
30      for i=2:N
```

```matlab
31          pc(i)=pc(i-1)+phi(i)*cos((i)*c);
32          qc(i)=qc(i-1)+phi(i)*sin((i)*c);
33      end
34
35      Vosc=zeros(ncut,1);
36
37      for n=1:ncut
38          Vosc(n)=Ephi*Ephi*( (1-cos(n*c))/(1-cos(c)) );
39      end
40
41      Mc=zeros(ncut,1);
42      Dc=zeros(ncut,1);
43
44      for n=1:ncut
45          MCpom=zeros(N-1-ncut,1);
46
47          MCpom(1)=(pc(1+n)-pc(1))^2+(qc(1+n)-qc(1))^2;
48
49          for j=1:N-1-ncut
50              MCpom(j+1)=MCpom(j)+(pc(j+n+1)-pc(j+1))^2+(qc(j+n+1)-qc(j+1))^2;
51          end
52
53          Mc(n)= MCpom(N-1-ncut)/(N-1-ncut);
54          Dc(n)=Mc(n)-Vosc(n);
55      end
56
57      CR=corrcoef(1:1:ncut,Dc);
58      Kc(m)=CR(2,1);
59
60  end
61
62  Kc; % result data
```

Listing 8.5: Matlab code for test for chaos 0-1.

9 Conclusion

In this work, a modification of the Fenton-Karma model of cardiac cell action potential is presented. Thanks to this modification, the resulting shape of the action potential is much better copied by the real data. In addition, the dynamic properties of this modified model were examined using the bifurcation diagrams, the Furier spectra, the Poincaré section, and the 0-1 test for chaos. The dynamics of investigated model (4.1, 4.4, 4.5) was analyzed in detail with respect to the amplitude A and stimulation delays c. The model was forced by stimulus with the shape of half-sine period. The equations of potentials were solved numerically using the Runge-Kutta method of the fourth order implemented as *ode45* solver in Matlab. It was observed that the model is showing regular (see, e.g., Figures 7.2 and 7.5) as well as irregular patterns (see Figure 7.6) for different range of stimulation delay and amplitude. This behavior of variables u, v, and w were also confirmed by bifurcation diagrams (Figure 7.7) and by the 0-1 test for chaos (Figures 7.9).

The results obtained were accepted for publication in the journal *Mathematical Methods in the Applied Sciences* ranking Q2 (108/255) in Mathematics, Applied (2016) with impact factor 1.017 (2016). Copy of this article can be seen in Appendix. In Section 8, there are matlab codes that were used to achieve the above mentioned results.

References

[1] Jaakko Malmivuo and Robert Plonsey. *Bioelectromagnetism - Principles and Applications of Bioelectric and Biomagnetic Fields.* 01 1995.

[2] E M Cherry and F H Fenton. Visualization of spiral and scroll waves in simulated and experimental cardiac tissue. *New Journal of Physics*, 10(12):125016, 2008.

[3] F Fenton and A Karma. Vortex dynamics in three-dimensional continuous myocardium with fiber rotation: Filament instability and fibrillation. *Chaos: An Interdisciplinary Journal of Nonlinear Science*, 8:20–47, 1998.

[4] World Health Organization. The top 10 causes of death. `http://www.who.int/mediacentre/factsheets/fs310/en/`, 2017. [Online; accessed 10-May-2018].

[5] L.S. Costanzo. *Physiology.* Saunders Text and Review Series. Saunders, 2002.

[6] R. H. Clayton, O. Bernus, E. M. Cherry, H. Dierckx, F. H. Fenton, L. Mirabella, A. V. Panfilov, F. B. Sachse, G. Seemann, and H. Zhang. Models of cardiac tissue electrophysiology: Progress, challenges and open questions. *Progress in Biophysics and Molecular Biology*, 104(1-3):22–48, 1 2011.

[7] R. FitzHugh. Impulses and physiological states in theoretical models of nerve membrane. *Biophys. J.*, 1:445–466, 1961.

[8] Willemijn Groenendaal, Francis A. Ortega, Armen R. Kherlopian, Andrew C. Zygmunt, Trine Krogh-Madsen, and David J. Christini. Cell-specific cardiac electrophysiology models. *PLOS Computational Biology*, 11(4):1–22, 04 2015.

[9] Robert A. Oliver and Wanda Krassowska. Reproducing cardiac restitution properties using the fenton–karma membrane model. *Annals of Biomedical Engineering*, 33(7):907–911, Jul 2005.

[10] Daniel M. Lombardo, Flavio H. Fenton, Sanjiv M. Narayan, and Wouter-Jan Rappel. Comparison of detailed and simplified models of human atrial myocytes to recapitulate patient specific properties. *PLOS Computational Biology*, 12(8):1–15, 08 2016.

[11] Paweł Derejko, Piotr Podziemski, Jan Jacek Żebrowski, Franciszek Walczak, and Łukasz Jan Szumowski. Effect of the restitution properties of cardiac tissue on the repeatability of entrainment mapping responseclinical perspective. *Circulation: Arrhythmia and Electrophysiology*, 7(3):497–504, 2014.

[12] STEFFAN PUWAL and BRADLEY J. ROTH. Numerical simulations of synchronized pacing. *Journal of Biological Systems*, 14(01):101–112, 2006.

[13] H Pak, Y Liu, H Hayashi, Y Okuyama, P Chen, and S Lin. Synchronization of ventricular fibrillation with real-time feedback pacing: implication to low-energy defibrillation. *American Journal of Physiology - Heart and Circulatory Physiology*, 285, 2003.

[14] D Allexandre and N Otani. Preventing alternans-induced spiral wave breakup in cardiac tissue: An ion-channel-based approach. *Phys. Rev. E*, 70, 2004.

[15] RH Clayton and AV Holden. Filament behavior in a computational model of ventricular fibrillation in the canine heart. *IEEE Transactions on Biomedical Engineering*, 51:28–34, 2004.

[16] Nagaiah Chamakuri, Christian Engwer, and Karl Kunisch. Boundary control of bidomain equations with state-dependent switching source functions in the ionic model. *Journal of Computational Physics*, 273(Supplement C):227 – 242, 2014.

[17] V Jacquemet. Steady-state solutions in mathematical models of atrial cell electrophysiology and their stability. *Mathematical Biosciences*, 208:241–269, 2007.

[18] David Nolte. The tangled tale of phase space. 63, 04 2010.

[19] Yuri A. Kuznetsov. *Elements of Applied Bifurcation Theory (2Nd Ed.)*. Springer-Verlag New York, Inc., New York, NY, USA, 1998.

[20] Francis C. Moon. *Chaotic and Fractal Dynamics: Introduction for Applied Scientists and Engineers*. Wiley-VCH, 1992.

[21] Davide Bernardini and Grzegorz Litak. An overview of 0–1 test for chaos. *Journal of the Brazilian Society of Mechanical Sciences and Engineering*, 38(5):1433–1450, Jun 2016.

[22] A Gottwald and I Melbourne. A new test for chaos in deterministic systems. *Proc. R. Soc. London A*, 460:603–611, 2004.

[23] A Gottwald and I Melbourne. On the implementation of the 0-1 test for chaos. *SIAM J. Appl. Dyn.*, 8:129–145, 2009.

[24] Georg A. Gottwald and Ian Melbourne. Testing for chaos in deterministic systems with noise. *Physica D: Nonlinear Phenomena*, 212(1):100 – 110, 2005.

[25] Christopher W. Kulp and Suzanne Smith. Characterization of noisy symbolic time series. *Phys. Rev. E*, 83:026201, Feb 2011.

[26] Matthew Nicol, Ian Melbourne, and Peter Ashwin. Euclidean extensions of dynamical systems. *Nonlinearity*, 14(2):275, 2001.

[27] Arkady S. Pikovsky, Michael A. Zaks, Ulrike Feudel, and Jürgen Kurths. Singular continuous spectra in dissipative dynamics. *Phys. Rev. E*, 52:285–296, Jul 1995.

[28] Tolga Yalç ınkaya and Ying-Cheng Lai. Bifurcation to strange nonchaotic attractors. *Phys. Rev. E*, 56:1623–1630, Aug 1997.

[29] Georg A Gottwald and Ian Melbourne. On the validity of the 0–1 test for chaos. *Nonlinearity*, 22(6):1367, 2009.

Appendix - Dynamical properties of the improved FK3V heart cell model

In the following, the original research article, that covers main results of this thesis, is enclosed. This paper was accepted for publication in the journal *Mathematical Methods in the Applied Sciences* ranking Q2 (108/255) in Mathematics, Applied (2016) with impact factor 1.017 (2016).

SPECIAL ISSUE PAPER

Dynamical properties of the improved FK3V heart cell model

Radek Halfar*[1,2] | Marek Lampart[1,3]

[1]VŠB - Technical University of Ostrava, Department of Applied Mathematics, Czech Republic

[2]VŠB - Technical University of Ostrava, Department of Cybernetics and Biomedical Engineering, Czech Republic

[3]VŠB - Technical University of Ostrava, IT4Innovations, Czech Republic

Correspondence
*Radek Halfar, VŠB - Technical University of Ostrava, 17. listopadu 15/2172, 708 33 Ostrava, Czech Republic. Email: radek.halfar@vsb.cz

Present Address
VŠB - Technical University of Ostrava, 17. listopadu 15/2172, 708 33 Ostrava, Czech Republic.

Abstract

The main aim of this paper is to study the evolution of the transmembrane potential on the cardiac cell under different rates and amplitudes of stimulation. For modeling this potential, the modification of the Fenton-Karma model was applied. It is a phenomenological model with three degrees of freedom that corresponds to non-dimensional transmembrane potential and gating variables for regulation of inward and outward ion currents which can better reproduce the shape of the transmembrane potential than the original Fenton-Karma model. The model was newly forced by stimulus with the shape of the half-sine period. As the main goal of the paper is to show that this model is showing regular as well as irregular motion; periodic as well as chaotic patterns are detected using bifurcation diagrams, the Fourier spectra, Poincaré sections, and 0-1 test for chaos.

KEYWORDS:
cardiac cell model, bifurcation, Fourier spectra, 0-1 test for chaos

1 | INTRODUCTION

The cardiac electrophysiology is the result of complex processes occurring on the heart cell membranes, which aim to ensure the proper progression of cardiac action potential inherent in the heart muscle. The stability of the propagation of the action potential in the heart tissue is often examined parameter[1,2,3]. The ordered propagation of the action potential is essential for the proper functioning of the heart, and a life-threatening condition, such as ventricular fibrillation, may occur when the propagation is not correct. To understand the dynamic properties of propagation of the action potential, it is important to examine not only the entire tissue but also the dynamic properties of the individual cells from which it is created.

The three variable Fenton-Karma (FK3V) model is commonly used to describe heart electrophysiology. Studies that use this model can be generally divided into several groups. Studies dealing with the determination of model parameters to better replicate the outputs obtained by using physiological models or experimental data, studies that uses the FK3V model to study the electrophysiology of the heart, and studies that examine the characteristics of the FK3V model itself.

The first group can include, for example, the study published by Oliver and Krassowska[4], which describes a procedure for finding such parameters of the FK3V model to its restitution characteristics corresponding to the restitution characteristics of the Courtemanche-Ramirez Nattel model of atrial tissue. Lombardo et al.[5] edited the parameters of the detailed model and FK3V to fit for five clinical data of patients undergoing ablation therapy.

Another possible field of study is termination of fibrillation[6]. Objective of this paper is to numerically validate the experimental techniques for terminating fibrillation presented in Pak et al.[7] In his work, they found that the synchronized defibrillation can create a low-energy alternative to the traditional defibrillation. Allexandre and Otani[1] studied the electrophysiological and dynamic mechanism of spiral wave break up. The authors found several alternans unstable modes with different growth rates,

---

[0]**Abbreviations:** FK3V, Three variable Fenton-Karma

frequencies and spatial structures. In another study[8], the authors examined the behavior of fibers in the computing FK3V monodomain anisotropic model of re-entrant ventricular fibrillation.

Another topic, which is often targeted in individual work dealing with the FK3V model, is the description of properties of the model itself. One of these studies examines the steady state of the system[2]. Linear stability of these points and their response to external stimulation were examined.

In this work an improvement of the FK3V model is introduced to obtain a better shape of action potential. The dynamical properties of this improved FK3V model are analyzed in dependence on the stimulation frequencies and amplitudes. It is shown that for suitable choices of the system parameters the system is chaotic (irregular patterns are visible) as well as periodic (regular).

For this purpose, the 0-1 test for chaos was applied. The 0-1 test for chaos, a newly established test[9,10], gives a binary characteristic of motion's behavior. More precisely, this test returns 0 for regular (periodic) and 1 for irregular (chaotic) patterns. The mathematical background can be found in the article by Gottwald and Melbourne[11], Bernardini and Litak[12] or in the latest review[13]. This test is applicable on discrete dynamical systems[14], continuous dynamical systems[15] as well as on a real data represented as time series[16]. This test has been successfully used in many applications, for example, in distinguishing between chaos and randomness from a noisy data[17], exploration of mechanical system's dynamic properties consisting of a ball jumping between a movable baseplate and a fixed upper stop[18]. This test was also used for analysis of the nonlinear floating potential fluctuations from a glow discharge plasma[19], for tracing the presence of nonlinearity and chaos in wireless network traffic[20], for chaos detection of the partial discharge patterns[21], or traffic flows[22].

The paper is organized as follows. In Section 2, the original FK3V model and its parameters are presented. Section 3 is dedicated to the model modification. In Section 4, the main results of this work are summarized. In particular, they include the phase portraits, Fourier spectra, and Poincaré section of the model results for various stimulation frequencies in Subsection 4.2, and test for chaos 0-1 for various stimulation frequencies and amplitudes in Subsection 4.3. The paper is closed by conclusions in Section 5.

2 | FK3V MODEL

The FK3V model is a dimensionless ionic model of cardiac action potential, which is based on the Luo-Rudy-I model. For reproducing action potential it uses three variables u, v, and w. Variable u represents the transmembrane potential (so that $u = 0$ and $u = 1$ are the rest and peak voltages, respectively). The transmembrane potential changes depending on ionic currents according to the following equation:

$$\dot{u} = J_{stim} - J_{fi} - J_{so} - J_{si} \tag{1}$$

where J_{fi} (accountable for depolarization of the membrane), J_{so} (accountable for repolarization of the membrane), and J_{si} (balances J_{so} during the plateau phase) are cross-membrane currents named fast inward (fi), slow outward (so), and slow inward (si) that roughly corresponds to sodium, potassium, and calcium ion currents, respectively. But because they do not represent the quantitatively measured currents but only their activation, inactivation, and reactivation, it is preferred to call these currents as fast and slow inward, and slow outward, rather than Na, Ca, and K as a reminder of these simplification. J_{stim} indicates the externally applied current. In this study, the external current composition of pulses is created by the first half period of sine function followed by zero function. J_{stim} is therefore defined by the following equation:

$$J_{stim} = \begin{cases} A\sin(t - n(c + 1)) & t \in [n(c + 1), n(c + 1) + 1] \ n \in \mathbb{N} \cup \{0\}, \\ 0 & t \notin [n(c + 1), n(c + 1) + 1] \ n \in \mathbb{N} \cup \{0\}, \end{cases} \tag{2}$$

where c denotes the length of time interval between pulses and A stands for the amplitude. In Equation 1 $\dot{u}$ denotes the first derivative of u with respect to time. The cross membrane currents are given by

$$J_{fi}(u; v) = \Theta(u - u_c)(1 - u)(u - u_c)\frac{-v}{\tau_d},$$

$$J_{so}(u) = \Theta(u_c - u)\frac{u}{\tau_0} + \Theta(u - u_c)\frac{1}{\tau_r}, \tag{3}$$

$$J_{si}(u; w) = \frac{-w(1 + \tanh(k(u - u_c^{si})))}{2\tau_{si}},$$

where $\Theta(x)$ is the Heaviside function.

Another two variables v and w used in the model are gating variables which regulate inactivation of J_{fi}, and J_{so} takes the following form:

$$\dot{v} = \Theta(u_c - u)(1 - v)\frac{1}{\tau_v^-(u)} - \Theta(u - u_c)v\frac{1}{\tau_v^+}, \tag{4}$$

$$\dot{w} = \Theta(u_c - u)(1 - w)\frac{1}{\tau_w^-} - \Theta(u - u_c)w\frac{1}{\tau_w^+}, \tag{5}$$

$\tau_v(u)$ is a function for defining the time constants for two voltage ranges ($u_v < u < u_c$ and $u < u_v$) and is introduced for proper reproducing CV restitution curve. It controls reactivation of J_{fi} and is given by equation

$$\tau_v^-(u) = \Theta(u - u_v)\tau_{v_1}^- + \Theta(u_v - u)\tau_{v_2}^-$$

The model contains several constants, which are used for fitting the output curves into the requested shape, time constants τ_r, τ_{si}, τ_0, threshold potentials u_c, u_c^{si}, and u_v.

The original paper[3] describes four different sets of parameters to fit for different dataset.

- BR: obtained by stimuli of the Beeler-Reuter model with standard parameter values.

- MBR: obtained by stimuli of modified the Beeler-Reuter model with accelerated up calcium kinetic.

- MLBR-I: stimuli of Luo-Rudy-I model with speeded up calcium kinetic.

- GP: experimental data from measuring the membrane potentials on the epicardial surface of the left Ventricle of a guinea pig.

TABLE 1 Original published parameters of the FK3V model[3] for BR parametric set, $k = 10$

Parameter	Description	unit	value
τ_d	setting influence J_{fi} for $u > u_c$	ms	0.25
τ_r	setting influence J_{so} for $u > u_c$	ms	33
τ_{si}	setting influence J_{si} on $\dot{u}$	ms	30
τ_0	setting decrease u to 0 for $u < u_c$	ms	12.5
τ_v^+	setting decrease v to 0 for $u > u_c$	ms	3.33
$\tau_{v_1}^-$	setting value for $\tau_v^-(u)$ for $u > u_v$	ms	1250
$\tau_{v_2}^-$	setting value for $\tau_v^-(u)$ for $u < u_v$	ms	19.6
τ_w^+	setting decrease w to 0 for $u > u_c$	ms	870
τ_w^-	setting increase w to 1 for $u < u_c$	ms	41
u_c	depolarization threshold	-	0.13
u_v	threshold for activation $\tau_{v_1}^-$ or $\tau_{v_2}^-$	-	0.04
u_c^{si}	threshold for opening J_{si}	-	0.85

3 | MODEL MODIFICATION

Since the shape of FK3V model is not realistic, the modification of this model is proposed. The modification consists of replacing constant τ_r in Equation 3 by the following function

$$\tau_r(u) = \Theta(u_{\tau_r} - u)\tau_r + \Theta(u - u_{\tau_r})\left(\frac{\tau_r(1 + \tanh(k_2(1 - u)))}{4} + \frac{\tau_r}{2}\right). \tag{6}$$

This equation divides $\tau_r(u)$ into two potential ranges. From 0 to u_{τ_r} where $\tau_r(u)$ remains constant and from u_{τ_r} above, where u decreases from τ_r to $\tau_r/2$. Another parameter introduced in Equation 6 is k_2 which sets the speed of decrease of $\tau_r(u)$. In this

work $u_{\tau_r} = 0.85$ and $k_2 = 20$. Another change from the original model is redefining u_c^{si} to value $u_c^{si} = 0.7$. The rest of the parameters stay the same as in the original BR parameters set (see Table 1).

In Figure 1 , the difference in the shape of the transmembrane potential of the original FK3V model as well as the modified model can be seen.
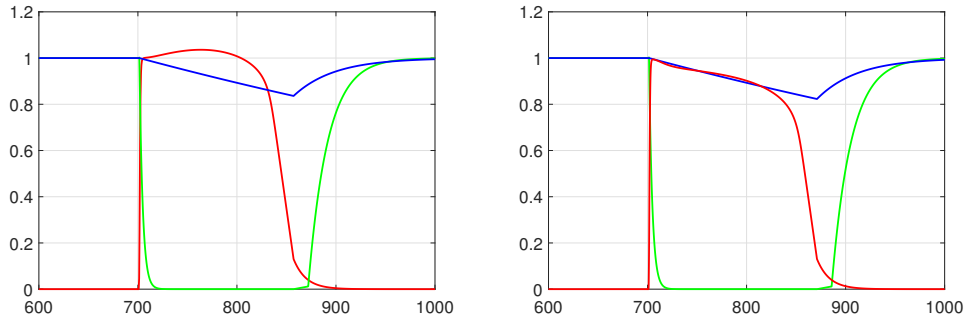

FIGURE 1 Time responses of u (red), v (green) and w (blue) of the original model (left) and improved model (right) for $c = 700$ ms and $A = 0.48$.

4 | MAIN RESULTS

In individual simulations, the heart cell was stimulated with the half-sine shaped current pulses with an amplitude from $A = 0.16$ to $A = 0.96$ with step of 0.04 and duration 1 ms. The individual stimulation pulses were separated by the delay c (see Equation 2). The computations were performed for the stimulation delays from 10 to 300 ms with step of 5 ms. Each simulation was done for the time from 0 to 5×10^5 ms. From the results, a phase diagram, amplitude frequency spectrum, and Poincaré section for each simulated frequency was computed. From the data was also created bifurcation diagram for the entire simulated frequency spectrum and the 0-1 test for chaos was computed.

4.1 | Phase portraits, the Fourier spectra, and Poincaré section

The Fourier spectra and phase portraits were computed for $A = 0.48$ (twice as needed to cause stimulation). Chaotic behavior of the model was observed on stimulation delays ranging from 30 to 50 ms and 105 ms. Regular behavior was observed elsewhere.

Cases with regular behavior can be divided into five groups (**RG1** – **RG5**). Each of these groups corresponds to the different biological response of the cell to the stimulatory pulses and corresponding representatives are shown in (Figure 2 – Figure 6); in all of these cases the Fourier spectra is formed by a number of harmonic frequencies, hence the frequency of the periodic trajectory is computable. Periodic motions of trajectories are also visible in Poincaré sections.

The irregular (chaotic) case is shown in Figure 7 , the **IRG** case. In this case, the Fourier spectra is formed by a number of harmonic components having the basic, super-harmonic, sub-harmonic, and combination frequencies on which there are superposed further motions with frequencies forming the sided bands of the dominant frequencies. Their mutual ratio indicates the irregularity of the motion. The character of this motion's case is underlined by the Poincaré section.

RG1 This case is represented in Figure 2) for stimulation delay 20 ms. The amplitude of u does not reach the full range (0 to 1), but changes only between 0 and 0.34. The action potential shape (variable u) also does not match with proper shape of action potential (see Figure 1 for comparsion).

RG2 At stimulation delays from 75 ms to 100 ms, stimulation causes every third stimulus (two unsuccessful stimulation followed by successful pacing). In the phase diagram, a closed loop with two spikes due to unsuccessful stimulation can be seen. The representative case of the model with this behavior can be seen in Figure 3 .
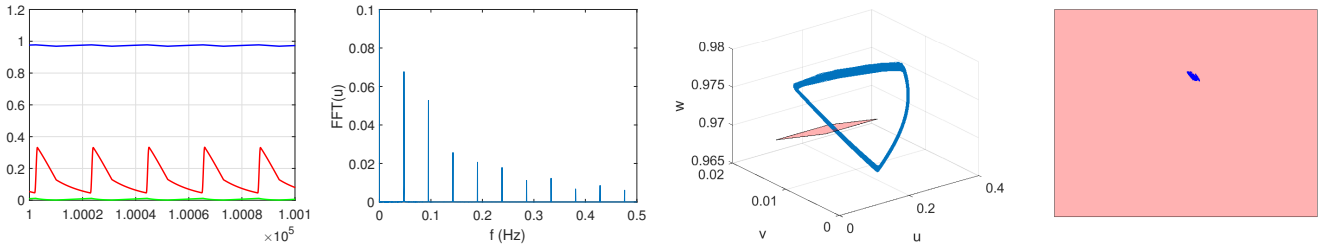
FIGURE 2 From the left: time responses of u (red), v (green), and w (blue); FFT of variable u; phase diagram and Poincaré section of the modified FK3V model for $c = 20$ ms.
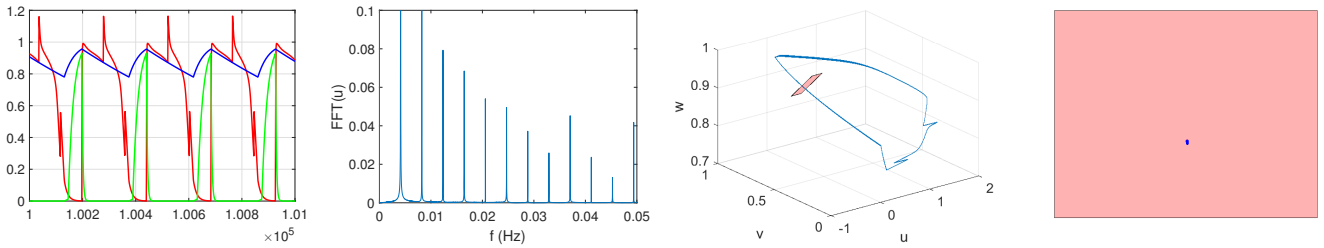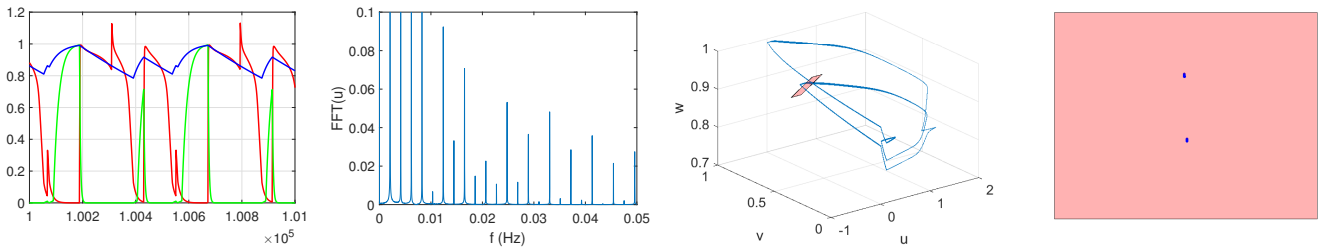

FIGURE 3 From the left: time responses of u (red), v (green), and w (blue); FFT of variable u; phase diagram and Poincaré section of the modified FK3V model for $c = 80$ ms.

FIGURE 4 From the left: time responses of u (red), v (green), and w (blue); FFT of variable u; phase diagram and Poincaré section of the modified FK3V model for $c = 120$ ms.

RG3 In Figure 4 , the typical model response for the delays ranging from 110 ms to 145 ms can be seen. The relevant stimulation is caused by every second stimulation impulse, but every second successful stimulation comes to phase of relative refracterity, therefore the action potential of this stimulation has shorter duration than the action potential of the previous successful stimulation impulse. In the phase portrait, two spikes from unsuccessful stimulation and two curves from the stimulation (one comes from the phase of relative refracterity and one comes from steady state) can be seen.

RG4 In Figure 5 , the representative case, every second stimulation impulse causes stimulation at delays from 150 ms to 185 ms. The action potential duration is about 200 ms.

RG5 Finally, in Figure 6 , the representative is shown where every stimulation impulse causes stimulation; this is observable for delays from 190 ms and above.

IRG The behavior of motions observed on delays from 30 ms to 50 ms and 105 ms is irregular, the representative can be seen in Figure 7 . In this case, the mutual ratio of stimulation impulse and stimulation indicates the irregularity of the motion. Moreover, these cases are chaotic due to the output of the 0-1 test for chaos performed in 4.3 Section.
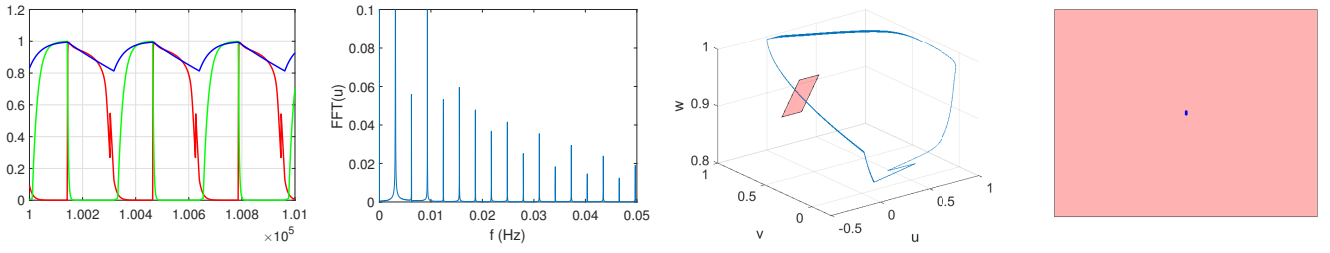
FIGURE 5 From the left: time responses of u (red), v (green), and w (blue); FFT of variable u; phase diagram and Poincaré section of the modified FK3V model for $c = 160$ ms.
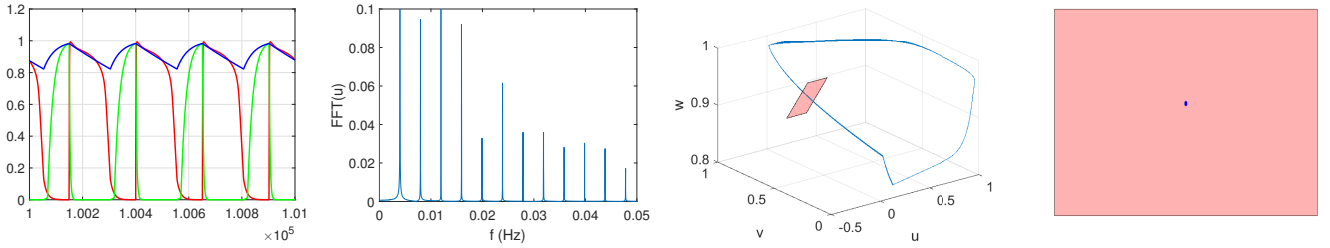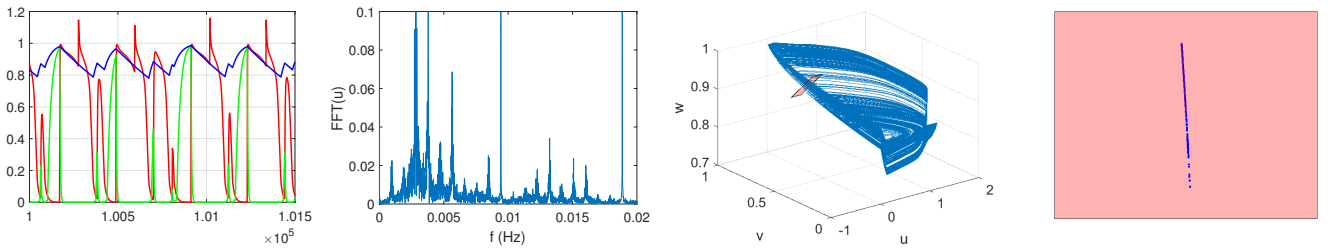

FIGURE 6 From the left: time responses of u (red), v (green), and w (blue); FFT of variable u; phase diagram and Poincaré section of the modified FK3V model for $c = 250$ ms.

FIGURE 7 From the left: time responses of u (red), v (green), and w (blue); FFT of variable u; phase diagram and Poincaré section the modified FK3V model for $c = 105$ ms.

4.2 | Bifurcation diagram

Next work was to plot bifurcation diagrams of modified FK3V model. Values for diagrams was collected witch period of stimulation frequency. Diagrams can be seen in Figure 8 . In diagrams can be seen, that stimulation delays from 30 to 50 ms and 105 ms are chaotic, at the other delays are regular responses. This coincides with time series exploration.

4.3 | The 0-1 test for chaos

Next, the 0-1 test for chaos was performed[9,10]. This test is used to distinguish regular and chaotic dynamics. It works with the time series and does not need any phase space reconstruction. The resulting value of this test can only be 0 (regular behavior) or 1 (chaos). This correlation method works as follows. For a given set of observations $\phi(j)$ for $j \in \{1, 2, \ldots, N\}$ are computed translation variables for suitable choice of $b \in (0, 2\pi)$.

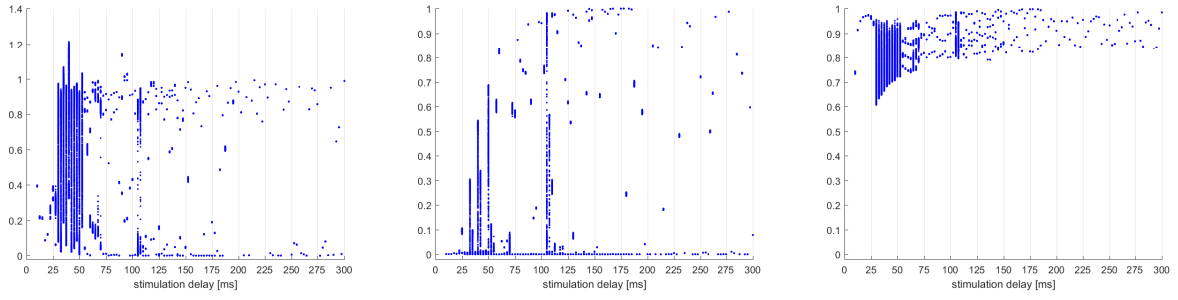$$p_b(n) = \sum_{j=1}^{N} \phi(j) \cos(jb) = 1,$$

FIGURE 8 Bifurcation diagram for variable u (left), v (middle), and w (right).
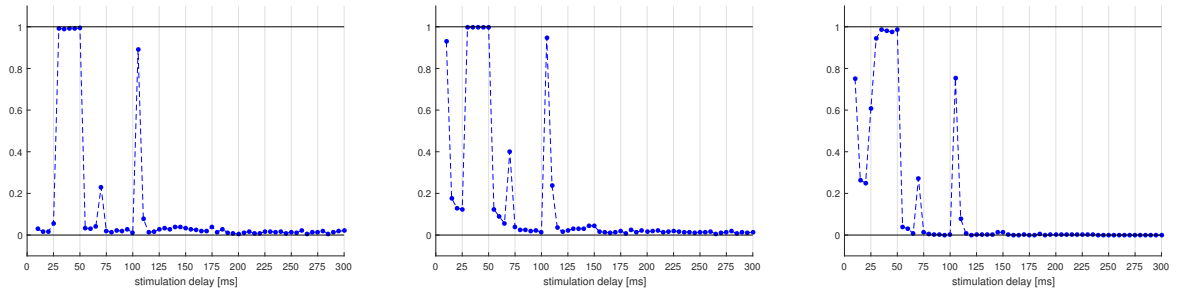

FIGURE 9 Results of the 0-1 test for chaos for $A = 0.48$ and c from 10 ms to 300 ms. Variable u (left), v (middle) and w (right).

$$q_b(n) = \sum_{j=1}^{N} \phi(j) \sin(jb) = 1,$$

then the mean square displacement is computed using the following equation

$$M_b(n) = \lim_{N \to \infty} \frac{1}{N} \sum_{j=1}^{N} [p_b(j + n) - p_b(j)]^2 + [q_b(j + n) - q_b(j)]^2$$

here $n \leq n_{cut}$ where $n_{cut} \ll N$. Then, the estimate of the modified mean square displacement is computed using the next equation

$$D_b(n) = M_b(n) - \left(\lim_{N \to \infty} \frac{1}{N} \sum_{j=1}^{N} \phi(j) \right)^2 \frac{1 - \cos(nb)}{1 - \cos(b)}.$$

Finally, the output of the 0-1 test is obtained as correlation coefficient of ξ and Δ for fixed parameter b

$$K_b = \mathrm{corr}(\xi, \Delta)$$

where $\xi = (1, 2, \ldots, n_{cut})$ and $\Delta = (D_c(1), D_c 2, \ldots, D_c(n_{cut}))$. Hence, K_b is dependent on the choice of c. To get K as the output of the 0-1 test, as limiting value of all K_b, the result value is taken as

$$K = \mathrm{median}(K_b).$$

The results of this test can bee seen in Figure 9 . At delays up to 25 ms, the behavior of variable u is regular, but for variables v and w , it cannot be decided if the behavior is chaotic or regular. Chaotic behavior of the model was observed on stimulation delays from 30 to 50 ms and 105 ms. There are also several cases of stimulation delays with the output of the 0-1 test for chaos in the range (0.1,0.9); in this cases it cannot be decided if it is chaotic or regular behavior, e.g. at the stimulation delay of 70 ms. Notice, that results of this test coincides with time series and bifurcation diagram.

But because of that, the stimulation of heart cell is dependent not only on the stimulation frequency but also on the amplitude of stimulation, the test for chaos 0-1 was computed also for the amplitude range from 0.16 to 0.96 in step 0.04. But since the results of the test for chaos 0-1 for $A = 0.48$ was the regular behavior for $c > 105$ ms (see Figure 9), the tests were computed
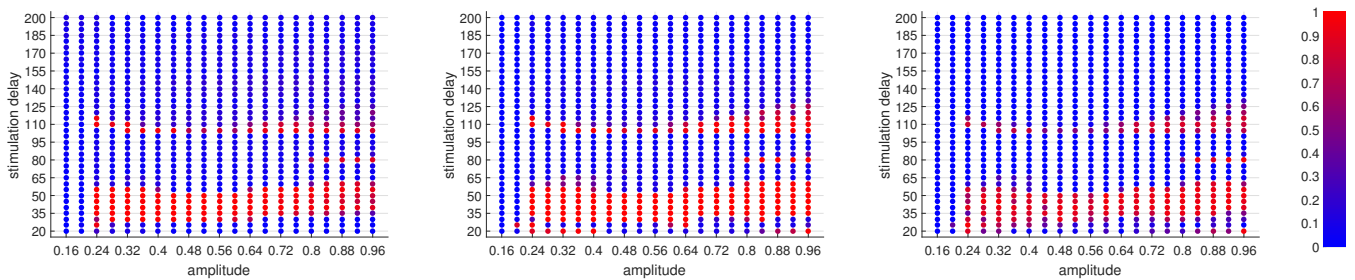
FIGURE 10 Results of the test for chaos 0-1 for various stimulation delays and amplitudes for variable (from the left) u, v, w and color bar (right).

for the stimulation delays from $c = 20$ ms to $c = 200$ ms in 5 ms increments. The results of this test can be seen in Figure 10 . From this figure can be seen that chaotic behavior is focused into three regions.

The first and biggest region of the chaotic behavior is at amplitudes from 0.24 above and stimulation delays from approximately 30 ms to 55 ms. Another area of section of chaotic behavior is at amplitudes from 0.8 and above and stimulation delay 80 ms. And the last region of chaotic behavior is at stimulation delay around $c = 105$ ms and amplitudes from $A = 0.24$.

5 | CONCLUSIONS

In this paper, the Fenton-Karma model of cardiac cell was improved and its dynamics was analyzed in detail with respect to the amplitude A and stimulation delays c. The model (1, 4, 5) was forced by stimulus with the shape of half-sine period. The equations of potentials were solved numerically using the Runge-Kutta method of the fourth order implemented as *ode45* solver in Matlab. It was observed that the model is showing regular (see, e.g., Figures 3 and 6) as well as irregular patterns (see Figure 7) for different range of stimulation delay and amplitude. For detection of this movements character, the Fourier spectra, Poincaré sections, and bifurcation diagrams (Figure 8) were used. Chaotic behavior of variables u, v, and w were confirmed by the 0-1 test for chaos (Figures 10), for suitable choices of stimulation delays and amplitudes.

References

1. Allexandre D, Otani N. Preventing alternans-induced spiral wave breakup in cardiac tissue: An ion-channel-based approach. *Phys. Rev. E.* 2004;70.

2. Jacquemet V. Steady-state solutions in mathematical models of atrial cell electrophysiology and their stability. *Mathematical Biosciences.* 2007;208:241–269.

3. Fenton F, Karma A. Vortex dynamics in three-dimensional continuous myocardium with fiber rotation: Filament instability and fibrillation. *Chaos: An Interdisciplinary Journal of Nonlinear Science.* 1998;8:20–47.

4. Oliver R, Krassowska W. Reproducing cardiac restitution properties using the Fenton-Karma membrane model. *Annals of Biomedical Engineering.* 2005;33:907–911.

5. Lombardo D, Fenton F, Narayan S, Rappel W. Comparison of detailed and simplified models of human atrial myocytes to recapitulate patient specific properties. *PLOS Computational Biology.* 2016;12:1–15.

6. Puwal S, Roth B. Numerical simulations of synchroniyed pacing. *Journal of Biological Systems.* 2006;14:101–112.

7. Pak H, Liu Y, Hayashi H, Okuyama Y, Chen P, Lin S. Synchronization of ventricular fibrillation with real-time feedback pacing: implication to low-energy defibrillation. *American Journal of Physiology - Heart and Circulatory Physiology.* 2003;285.

8. Clayton RH, Holden AV. Filament behavior in a computational model of ventricular fibrillation in the canine heart. *IEEE Transactions on Biomedical Engineering.* 2004;51:28–34.

9. Gottwald A, Melbourne I. A new test for chaos in deterministic systems. *Proc. R. Soc. London A.* 2004;460:603–611.

10. Gottwald A, Melbourne I. On the implementation of the 0-1 test for chaos. *SIAM J. Appl. Dyn..* 2009;8:129–145.

11. Gottwald Georg A, Melbourne Ian. On the validity of the 0-1 test for chaos. *Nonlinearity.* 2009;22(6):1367.

12. Bernardini Davide, Litak Grzegorz. An overview of 0–1 test for chaos. *Journal of the Brazilian Society of Mechanical Sciences and Engineering.* 2015;38(5):1433–1450.

13. Gottwald Georg A., Melbourne Ian. The 0-1 Test for Chaos: A Review. In: Springer Berlin Heidelberg 2016 (pp. 221–247).

14. Lampart Marek, Martinovič Tomáš. A survey of tools detecting the dynamical properties of one-dimensional families. *Advances in Electrical and Electronic Engineering.* 2017;15(2):304-313.

15. Melosik M., Marszalek W.. On the 0/1 test for chaos in continuous systems. *Bulletin of the Polish Academy of Sciences Technical Sciences.* 2016;64(3).

16. Falconer Ian, Gottwald Georg A., Melbourne Ian, Wormnes Kjetil. Application of the 0-1 Test for Chaos to Experimental Data. *SIAM Journal on Applied Dynamical Systems.* 2007;6(2):395-402.

17. Kulp Christopher W., Smith Suzanne. Characterization of noisy symbolic time series. *Phys. Rev. E.* 2011;83:026201.

18. Lampart Marek, Zapoměl Jaroslav. Dynamical properties of a non-autonomous bouncing ball model forced by non-harmonic excitation. *Mathematical Methods in the Applied Sciences.* 2016;39(16):4923–4929. mma.4186.

19. R. Chowdhury D, N. S. Iyengar A, Lahiri S. Gottwald Melborune (0-1) test for chaos in a plasma. 2012;19:53-56.

20. Mukherjee Somenath, Ray Rajdeep, Samanta Rajkumar, Khondekar Mofazzal H., Sanyal Goutam. Nonlinearity and chaos in wireless network traffic. *Chaos, Solitons & Fractals.* 2017;96:23 - 29.

21. Lampart Marek, Vantuch Tomáš, Zelinka Ivan, Mišák Stanislav. Dynamical properties of partial-discharge patterns. *International Journal of Parallel, Emergent and Distributed Systems.* 2017;0(0):1-16.

22. Martinovič Tomáš. Chaotic behaviour of noisy traffic data. *Mathematical Methods in the Applied Sciences.* 2016;:n/a–n/a. mma.4234.

□